Atmos. Chem. Phys. Discuss., 8, 13063–13123, 2008
www.atmos-chem-phys-discuss.net/8/13063/2008/

Atmospheric Chemistry and Physics Discussions

Comparison of CMAM simulations of carbon monoxide (CO), nitrous oxide (N_2O), and methane (CH_4) with observations from Odin/SMR, ACE-FTS, and Aura/MLS

J. J. Jin[1], K. Semeniuk[1], S. R. Beagley[1], V. I. Fomichev[1], A. I. Jonsson[2], J. C. McConnell[1], J. Urban[3], D. Murtagh[3], G. L. Manney[4,5], C. D. Boone[6], P. F. Bernath[6,7], K. A. Walker[2,6], B. Barret[8], P. Ricaud[8], and E. Dupuy[6]

[1]Department of Earth and Space Science and Engineering, York University, Toronto, Ontario, Canada
[2]Department of Physics, University of Toronto, Ontario, Canada
[3]Department of Radio and Space Science, Chalmers University of Technology, Goteborg, Sweden
[4]Jet Propulsion Laboratory, California Institute of Technology, Pasadena, California, USA
[5]New Mexico Institute of Mining and Technology, Socorro, New Mexico, USA
[6]Department of Chemistry, University of Waterloo, Waterloo, Ontario, Canada

[7]Department of Chemistry, University of York, Heslington, York, UK
[8]Laboratoire d'Aérologie, UMR 5560 CNRS/Université Paul Sabatier, Observatoire de Midi-Pyrénées, Toulouse, France

Received: 9 May 2008 – Accepted: 9 June 2008 – Published: 9 July 2008

Correspondence to: J. J. Jin (jin@nimbus.yorku.ca)

Published by Copernicus Publications on behalf of the European Geosciences Union.

Abstract

Simulations of CO, N_2O and CH_4 from a coupled chemistry-climate model (CMAM) are compared with satellite measurements from Odin Sub-Millimeter Radiometer (Odin/SMR), Atmospheric Chemistry Experiment Fourier Transform Spectrometer (ACE-FTS), and Aura Microwave Limb Sounder (Aura/MLS). Pressure-latitude cross-sections and seasonal time series demonstrate that CMAM reproduces the observed global distributions and the polar winter time evolutions of the CO, N_2O, and CH_4 measurements quite well. Generally, excellent agreement with measurements is found in CO monthly zonal mean profiles in the stratosphere and mesosphere for various latitudes and seasons. The difference between the simulations and the observations are generally within 30%, which is comparable with the difference between the instruments in the upper stratosphere and mesosphere. In general, the CO measurements also show an excellent agreement between themselves although MLS retrievals are noisier than other retrievals above 10 hPa (~32 km). The measurements also show large difference in the lower stratosphere and upper troposphere. Comparisons of N_2O show that CMAM results usually have a less than 15% difference to the measurements in the lower and middle stratosphere, and the observations are consistent as well. However, the standard version of CMAM has a serious low bias in the upper stratosphere. The CMAM CH_4 distribution is also close to the observations in the lower stratosphere, but has a similar but smaller negative bias in the upper stratosphere. These negative biases can be reduced by introducing a vertical diffusion coefficient related to gravity wave drag. CO measurements from 2004 and 2006 show evidence of enhanced descent of air from the mesosphere into the stratosphere in the Arctic after strong stratospheric sudden warmings (SSWs). CMAM also shows strong descent of air after SSWs, but further investigation is needed. In the tropics, CMAM captures the "tape recorder" (or annual oscillation) in the lower stratosphere and the semiannual oscillations (SAO) at the stratopause and mesopause shown in MLS CO and SMR N_2O observations. The inter-annual variation of the SAO at the stratopause in SMR N_2O

ACPD

8, 13063–13123, 2008

observations also shows a biennial oscillation, but CMAM cannot does not reproduce this feature. However, this study confirms that CMAM is able to simulate middle atmospheric transport processes reasonably well.

1 Introduction

The Canadian Middle Atmosphere Model (CMAM) is a coupled Chemistry-Climate Model (CCM) and incorporates comprehensive representations of the middle atmospheric radiation, dynamics, and chemistry as well as standard processes for tropospheric general circulation models (GCMs) (Beagley et al., 1997; de Grandpré et al., 2000; Fomichev et al., 2004). The model has been extensively used to investigate middle atmospheric climate change (i.e. Jonsson et al., 2004; Fomichev et al., 2007), conduct data assimilation (Polavarapu et al., 2005), and assess changes to the global ozone layer (WMO, 2003, 2007; Eyring et al., 2006, 2007; Shepherd and Jonsson, 2008). A previous model assessment showed that the model ozone climatology agrees well with observations (de Grandpré et al., 2000). This was also confirmed in a more recent assessment (Eyring et al., 2006) where a limited set of temperature, ozone (O_3), water vapour (H_2O), methane (CH_4) and hydrogen chloride (HCl) measurements and age of air estimates were compared with simulations from over a dozen CCMs. This comparison, which was focused on model comparisons rather than extensive measurement comparisons, also suggested that CMAM is representative of the better-performing models. In this paper, we perform a much more extensive and challenging comparison of CMAM with measurements. In particular, CMAM results for carbon monoxide (CO), nitrous oxide (N_2O) and CH_4 are compared with observations from three satellite instruments: Atmospheric Chemistry Experiment Fourier Transform Spectrometer (ACE-FTS), Odin Sub-Millimeter Radiometer (Odin/SMR) and Aura Microwave Limb Sounder (Aura/MLS). This allows us to evaluate chemistry and transport processes in the model, while the inter-comparison between the measurements allows us to further evaluate the quality of the observational data after the recent validation

ACPD
8, 13063–13123, 2008

studies on CO (Barret et al., 2006; Clerbaux et al, 2008; Pumphrey et al., 2007; Livesey et al., 2008), N_2O (Lambert et al., 2007; Strong et al., 2008) and CH_4 (De Mazière et al., 2008).

CO, N_2O and CH_4 have local chemical lifetimes in the middle atmosphere that are equivalent to or longer than the typical advection and mixing timescales, and thus they act as useful tracers for middle atmospheric transport processes (e.g. Brasseur and Solomon, 2005). CO in the middle atmosphere is mainly produced by oxidation of CH_4 in the stratosphere and by photolysis of CO_2 in the mesosphere and thermosphere, and is mainly destroyed through the reaction with hydroxyl radicals (OH). The local chemical lifetime of CO is about six months in the lower stratosphere and three weeks in the upper stratosphere. It increases to about two months in the lower mesosphere. In the upper mesosphere the local lifetime can be over one year and becomes even longer in the thermosphere. In addition, there is virtually no chemical loss during polar night because of the absence of OH in those regions. N_2O is emitted at the surface of the Earth and its local chemical lifetime varies from years in the lower stratosphere to weeks in the upper stratosphere and mesosphere. N_2O is primarily destroyed by photolysis; however, the oxidation of N_2O through the reaction with excited oxygen atoms ($O(^1D)$) is the main source of stratospheric nitrogen oxides (NO_x=NO+NO_2). CH_4 is also emitted at the Earth's surface and is destroyed through reactions with OH and $O(^1D)$ producing CO and H_2O in the middle atmosphere. It also reacts with atomic chlorine to produce HCl. CH_4 has a local chemical lifetime ranging from over 100 yrs in the lower stratosphere to months in the middle stratosphere. Its lifetime increases to a few years at the stratopause, but decreases again above that, ranging from weeks to days above 70 km due to photolysis by Lyman-α radiation. It can be seen that the middle atmospheric N_2O and CH_4 are transported from the surface and their volume mixing ratios (VMRs) decrease with height. Middle atmospheric CO, while produced locally, is still subject to transport processes and its VMR increases with height. Hence, these three species allow us to test different dynamical aspects of the model.

The SMR on board the Odin satellite performs limb observations of trace gases in the

spectral range 486–581 GHz (Murtagh et al., 2002). CO is retrieved from the 576.6 GHz band between ~18–100 km with an altitude resolution of about 3 km. The retrieval methodology of CO is described by Dupuy et al. (2004). N_2O is retrieved from a line at 502.3 GHz in the altitude range 13–50 km with a vertical resolution of 1.5–2 km (Urban et al., 2005, 2006). ACE-FTS is a Fourier Transform Spectrometer on the Canadian Atmospheric Chemistry Experiment (ACE) satellite SCISAT-1 (Bernath et al., 2005). It currently measures temperature, pressure and more than thirty species involved in ozone-related chemistry as well as isotopologues of some of the molecules. ACE-FTS observes solar occultations in the spectral range 750–4400 cm^{-1} (2.3–13.3 μm) with a high spectral resolution of 0.02 cm^{-1}. The vertical resolution is ~3–4 km. The retrieval approach for temperature, pressure, and volume mixing ratios is described by Boone et al. (2005). Information on the CO retrievals can also be found in Clerbaux et al. (2005).

We also compare the model simulations with measurements from the MLS (Waters et al., 2006) on the Aura satellite. The MLS CO data are retrieved from the measurements of the 240 GHz radiometer with a vertical resolution of about 2.5 km in the stratosphere and mesosphere and about 4 km in the upper troposphere and lower stratosphere (Pumphrey et al., 2007; Livesey et al., 2008). The N_2O measurements are derived from the 640 GHz retrievals with a vertical resolution of about 4–5 km between 100–1 hPa (Lambert et al., 2007).

Recent comparisons between these instruments show that the measurements for CO, N_2O and CH_4 are reliable (Barret et al., 2006; Clerbaux et al, 2008; De Mazière et al., 2008; Lambert et al., 2007; Livesey et al., 2008; Pumphrey et al., 2007; Strong et al., 2008). The difference between ACE-FTS and SMR CO measurements is less than 25% between 25–68 km, but ACE-FTS CO is about 50% lower than the CO from SMR below 22 km. Compared to MLS, the ACE-FTS CO is significantly lower in the troposphere, up to 50% higher in the lower stratosphere, and about 25% lower in the mesosphere. MLS CO is noisier than CO from ACE-FTS and SMR (Clerbaux et al., 2008; Pumphrey et al., 2007). The MLS N_2O measurements are close to the ACE-FTS and SMR data, generally within 5–10% difference between 100–1 hPa (Strong et

al., 2008). The agreement between ACE-FTS and SMR is also excellent below 40 km where the difference is generally less than 10% on average. The relative agreement becomes worse above 40 km because of decreasing N_2O mixing ratios with altitude albeit a small absolute difference of 2–3 ppbv between the N_2O data of the two instruments (Lambert et al., 2007; Strong et al., 2008). De Mazière et al. (2008) show that the ACE-FTS CH_4 also has a generally good agreement with other observations but has a 5–20% positive bias between 10 and 55 km compared to measurements from the Halogen Occultation Experiment (HALOE) on board the Upper Atmosphere Research Satellite (UARS).

An earlier inter-comparison of CO showed good agreement between ACE-FTS and Odin/SMR at various latitudes and seasons, and good agreement between these measurements and CMAM simulations at low latitudes as well as poor agreement between the measurements and model results in the polar winter stratosphere (Jin et al., 2005). The poor agreement was due to the typically abnormal meteorological condition for the Arctic winter 2004 (Manney et al., 2005a) and the large background vertical diffusion coefficient ($1.0\,m^2\,s^{-1}$) used in the model at that time. That coefficient has now been reduced and the model's performance has generally improved, particularly in the lower and middle stratosphere. In this study, we compare observations from three instruments which have different properties: ACE-FTS observations have precise profiles and MLS measurements have a global coverage while the SMR observations have not only a global coverage but also a longer time record, as described in Sect. 2.

In Sect. 2, the CMAM simulation and the processing of the measurements from the instruments are described. The comparisons of CO, N_2O, and CH_4 are presented in Sects. 3, 4 and 5, respectively. The time evolution of the measurements and the model results in the polar regions are analyzed in Sect. 6. The enhanced Arctic upper stratosphere and lower mesosphere descent associated with stratospheric sudden warmings in 2004 and 2006, which has been highlighted in recent studies (Randall et al., 2006; Manney et al., 2008a, 2008b), is also discussed in this section. To our knowledge this is the first time that the complete annual evolution of CO in the stratosphere and

ACPD
8, 13063–13123, 2008

mesosphere in the Arctic and Antarctica is shown. In Sect. 7, the annual and inter-annual oscillations in satellite measurements and model simulation in the tropics are compared. Section 8 provides a summary of this study.

2 CMAM simulation and measurement

This study uses the standard version of CMAM which has a spectral horizontal resolution of T31 with an associated horizontal grid of 64×32 points (5.8°×5.8°). There are 71 vertical levels and the upper boundary is at 6×10^{-4} hPa (~95 km geometric altitude). The standard version of the model used in this study includes comprehensive stratospheric gas phase and heterogeneous chemistry, but tropospheric chemistry is limited and detailed surface emissions are not included in the model. Additional details are given in de Grandpré et al. (2000). In the simulation, the surface concentrations of green house gases CO_2, CH_4 and N_2O are based on the Intergovernmental Panel on Climate Change (IPCC) (2001). In addition, the quasi-biennial oscillation in the tropical stratospheric zonal wind is neither internally generated nor externally driven by observed equatorial zonal wind. Details of the particular simulation used for the comparisons herein are given in Eyring et al. (2006) and we used the data for the period of 2004–2007.

For comparison, the ACE-FTS, SMR and MLS retrievals are first binned into latitudinal bands centered on the CMAM grid and interpolated to the CMAM pressure levels. Monthly and seasonal zonal averages are calculated from the gridded datasets. In order to reduce the noise in the SMR and MLS CO retrievals, however, running averages in 10 degree-wide latitude bands, centered at the CMAM latitude grid points, are used in the CO cross-section Figs. 1 and 12. For ACE-FTS, Vers. 2.2 retrievals for the period February 2004 to August 2007 are used. Validation studies, in addition to the work introduced in Sect. 1, can be found in the special issue on "Validation results for the Atmospheric Chemistry Experiment" in Atmospheric Chemistry and Physics (2008). The observational geometry of the ACE-FTS instrument is such that up to 15 sunrise

ACPD
8, 13063–13123, 2008

and 15 sunset observations are collected along two latitude circles per day. One of the circles of nearly constant latitude is in the Northern Hemisphere and the other is in the Southern Hemisphere. The observed latitudes vary with time so that over several months global coverage is achieved. We note that this distribution of occultations means that the temporal coverage for some latitude bins and months is limited. As a result, only the CMAM zonal means sampled at the nearest latitudes to the ACE-FTS locations on the simulation day, rather than the whole CMAM results in the latitudinal and seasonal bins, are applied in the comparisons with the ACE-FTS seasonal profiles in Sects. 3, 4, and 5.

SMR and MLS both provide measurements with near-global coverage, between 82.5° S and 82.5° N. The observation time for SMR was divided between aeronomy and astronomy, but the astronomical observations ceased in April 2007 and the SMR is now used solely for aeronomical observations. For SMR, the results from the latest CO retrievals, Vers. 225, between October 2003 and August 2006, and the Vers. 2.1 N_2O between July 2001 and February 2007 are used. We use the N_2O data with the quality flags of 0 or 4 and CO data with the quality flags of 0. For both molecules, we only use data with measurement responses greater than 0.9 (see Urban et al. (2005) for a description of the quality flag and the measurement response). In contrast to N_2O, CO measurements are conducted only on about 1–2 d per month (see Table 1), which likely introduces biases in the derived monthly averages compared to mean atmospheric conditions. However, we estimate that this error is small considering the long local chemical lifetime of CO in the atmosphere, as noted above, except at the middle and polar latitudes where fast meridional and vertical transport affects the CO distribution in winter.

For MLS, we use the new Vers. 2.2 retrievals between August 2004 and March 2008. The processing and validation of this new version of the data can be found in a special section on "Aura Validation" in Journal of Geophysical Research (Vol. 112(D24), 2007).

3 CO comparisons

3.1 Monthly zonal mean cross-sections

Figure 1 shows monthly and zonal mean CO latitude-pressure cross-sections of the simulation and the observations above 400 hPa in January, April, July, and October. Since the SMR observations currently are available only for limited time periods (particularly during 2004, see Table 1), we use data from January 2004 and January 2006, April 2004, July 2004, and October 2003 for the monthly averages in January, April, July, and October, respectively. However, all other observations and the model simulation are multi-year averages for the four months. It can be seen that the CMAM simulation generally agrees well with the measurements throughout the model domain for the four seasons. A detailed comparison follows.

The model simulation and the observations show large and comparable CO mixing ratios in the mesosphere. The CO mixing ratio generally increases from ~0.1 ppmv in the lower mesosphere to about 10–50 ppmv in the upper mesosphere. This strong increase with altitude in the mesosphere is caused by the increasing photolysis of CO_2, and the relatively constant or increasing local chemical lifetime against the loss reaction with OH. There is also a strong meridional gradient from the summer polar region to the winter polar region in the mesosphere, reflecting both chemistry and dynamics. From a photochemistry perspective, the CO photochemical source and the variation of local chemical lifetime from about 30 d in polar daylight regions to tens of years in polar night regions are important factors involved. The single-cell structure of the meridional circulation from the summer hemisphere to the winter hemisphere in the mesosphere (Andrews et al., 1987) is another factor affecting the meridional gradient.

A downward extension of the high mesospheric CO values into the upper stratosphere at high latitudes in winter is evident both in the CMAM results and in the ACE-FTS, SMR and MLS observations. For the northern high latitudes, the 0.1 ppmv contour in the CMAM and the MLS data descends from about 0.5 hPa in October to about 10 hPa in January (corresponding to a descent rate of about 7 km per month) and a

ACPD
8, 13063–13123, 2008

similar downward movement can be seen at southern high latitudes from April to July (7 km per month). A strong CO meridional gradient in the winter polar region and associated downward transport have been reported in observations by ISAMS (Allen et al., 2000), SMR (Dupuy et al., 2004) and MLS (Pumphrey et al., 2007). The ISAMS observations showed a similar descent rate (about 7.5 km per month) in the Antarctic upper stratosphere and lower mesosphere from late April to late July (Allen et al., 2000). SMR observations show a stronger CO enhancement in the Antarctic middle stratosphere in July than in the Arctic middle stratosphere in January. In the MLS data, between about 2 and 0.1 mb, the 0.5 ppmv contour is farther from the pole and also lower in the Antarctic stratosphere in July than in the Arctic stratosphere in January showing stronger CO enhancement in a broader region in the Antarctica than in the Arctic during winter. This feature is also well reproduced by the model, and can be attributed to the less disturbed nature of the southern winter vortex.

The observed enhancement of CO in the middle and upper stratosphere between 10–1 hPa (~32–50 km) in the tropics is due to CH_4 oxidation in rising air in this region (Allen et al., 1999) and is clearly captured by the model. The enhancement displays a seasonal variation in the model simulation between 5–1 hPa (~38 km–50 km), being notably weaker in January and July than in April and October. This is due to the Semiannual Oscillation (SAO), which will be discussed in Sect. 7. Briefly, the CO variation is caused by a combination of upward transport of CH_4 and its oxidation. However, it is difficult to see this seasonal variation in the measurements due to the discontinuous record of the ACE-FTS tropical retrievals and due to the noise in the SMR and MLS data.

The CMAM produces very small CO mixing ratios (less than 15 ppbv) around 5 hPa in the Antarctic middle stratosphere in April and in the Arctic middle stratosphere in October, and in the lower tropical stratosphere (around 50 hPa, 20 km) in all seasons. These small CO values are also observed by the satellite instruments although SMR and MLS are somewhat noisier than ACE-FTS. The polar minimum is due to the combination of chemical loss by OH, reduced production from CH_4, and reduced meridional

transport from lower latitudes. The lower tropical stratosphere minimum represents the turning point between two regions of CO production: fossil fuel and biomass burning in the troposphere and chemical production from CH_4 in the stratosphere. In addition, MLS has a significant negative bias in the lower stratosphere (around 30 hPa) (Pumphrey et al., 2007), which will be shown more clearly in Figs. 2 and 3.

One significant difference between CMAM and the observations is the larger modeled CO maximum compared to the MLS and SMR observations near the South Pole between 20–10 hPa in October. This discrepancy is also present in November (not shown), and reflects a common problem with current CCMs, which tend to have a cold bias in the austral spring and a later break-up of the Antarctic polar vortex than what is observed (Shepherd, 2000; Eyring et al., 2006).

The measurements from the three instruments display similar distributions throughout the domain and seasons, except that the CO from SMR is obviously smaller than that from MLS above the middle stratosphere (above 10 hPa) in the Arctic in January. This disagreement can be attributed to the different meteorological conditions in the datasets: The SMR averages are the means of the observations in January 2004 and 2006 when the Arctic stratospheric vortices were not strong (see details in Sect. 6). The MLS averages are the means of observations in January between 2005 and 2008, while the stratospheric vortices in January 2005 and 2007 were very strong (Manney et al., 2006; Rösevall et al., 2007). The meteorological data (not shown) show that the Arctic stratospheric vortex was also strong in January 2008.

3.2 Seasonal zonal mean profiles

Figure 2 shows model and observed seasonal zonal mean CO profiles in the latitudinal bands 90° S–60° S, 60° S–20° S, 20°–20° N, 20° N–60° N, and 60° N–90° N for December–January–February (DJF), March–April–May (MAM), June–July–August (JJA), and September–October–November (SON). The ratios of the observations to the CMAM results are shown in Fig. 3. Figure 3 also shows the ratios of the CMAM zonal means sampled near the ACE-FTS latitudes to the CMAM zonal means at the full

latitude bands. If these ratios (CMAM sampled near the ACE-FTS latitudes)/CMAM depart far from 1, the averages of the values sampled near the ACE-FTS latitudes cannot represent the averages at the full latitude bands. However, only in the polar regions in the winter season (in the Antarctica for JJA and the Arctic for DJF) is there a noticeable difference between the CMAM zonal means at the full latitude bands and the values at the ACE-FTS latitudes (see Fig. 2) and a noticeable departure of the ratios from 1 (see Fig. 3). That means that the mean ACE-FTS values are comparable to the CMAM values except in these regions. Nevertheless, we note that the ACE-FTS/CMAM ratios are derived from the ACE-FTS zonal means and the CMAM zonal means sampled near the ACE-FTS latitudes, so that the effect of the varying ACE-FTS locations on the comparison can be eliminated.

The seasonal zonal mean observations generally are in good agreement in the upper stratosphere and mesosphere above about 10 hPa (~32 km), as was already suggested in the cross-sections in Fig. 1. All the instrument profiles show similar meridional trends, with CO increasing from the summer polar region to the winter polar region. However, there are some discrepancies among the observations in the upper stratosphere and mesosphere. The SMR observations generally show a negative bias compared to ACE-FTS and MLS in the mesosphere, especially in the Antarctica above 0.1 hPa for June–August and in the Arctic above 10 hPa for December–February.

CMAM reproduces the observations reasonably well in the upper stratosphere and mesosphere (above 10 hPa, see Fig. 3), where the CMAM CO follows the observations closely over 3 orders of magnitude. CMAM also reproduces the meridional trend and the seasonal cycle demonstrated by the measurements. However, CMAM has a positive bias of CO between 1–0.01 hPa (about 50–80 km) in the tropics for all seasons. At middle and high latitudes, CMAM also shows a slight over-estimation, but the bias varies with altitude and season.

A step-like feature can be seen both in the model results and in the observations at 10 hPa over Antarctica in the austral winter (June–August). This feature is the result of the descent of CO-rich air from the mesosphere in the polar vortex. In the austral

spring (September–November) a local maximum near 10 hPa, which is the remnant of the CO-rich air in the Antarctic vortex, and a local minimum above it, which is due to the dilution of mid-latitude low-CO air in the breaking upper stratospheric vortex, are also reproduced by CMAM. However, the simulated local maximum is larger than the observations, which is also shown in the cross-sections in Fig. 1 and is discussed in Sect. 3.1. This is likely due to the late break-up of the model Antarctic vortex.

Between 100–10 hPa (~16–32 km) CMAM shows good agreement with ACE-FTS. Both profiles show local minima (<20 ppbv) near 50 hPa in the tropics and near 100 hPa in the polar regions. These minima reflect the turning point previously discussed. The MLS observations show a negative bias and the SMR observations show a positive bias compared to ACE-FTS. The largest negative bias for MLS occurs near 30 hPa, which is consistent with the MLS systematic negative bias in the lower stratosphere (Pumphrey et al., 2007). This negative bias is most severe in the tropics but less noticeable in the polar regions.

In the upper troposphere, CMAM values are similar to ACE-FTS values in the southern polar region, but are smaller than the ACE-FTS values at other latitudes, particularly in the northern hemisphere. However, we note that CMAM does not include detailed tropospheric surface emissions: the only tropospheric CO source is from CH_4 oxidation. Furthermore, the CMAM CO surface boundary condition used for this simulation is set to a constant value of 50 ppbv, which is far from the real surface values varying from a minimum 35–45 ppbv in the southern summer to a maximum 200–210 ppbv in the northern winter (Brasseur and Solomon, 2005). Moreover, the MLS and ACE-FTS observations show discrepancies in the upper troposphere, consistent with recent validation results showing that MLS has a persistent positive bias by a factor of 2 in the upper troposphere, although the morphology is realistic for scientific use (Livesey et al., 2008).

The relative differences between the observations and the simulation vary significantly in the vertical, but the ratios generally are within 0.7–1.3 in the stratosphere and mesosphere (see Fig. 3). In general, CMAM values are about 20% larger than those

ACPD
8, 13063–13123, 2008

from ACE-FTS and about 50% larger than values from SMR, while the relative difference with respect to MLS lies between these two values above 1 hpa (~50 km). The over-estimation is probably due to that the VMR of CO_2 is fixed in the standard version of CMAM, which results in more CO source than in the real atmosphere. Between 10 hPa and 1 hPa, CMAM is closer to ACE-FTS and SMR than to MLS, which shows a positive bias up to 50%, as stated above. Between 100–10 hPa, the CMAM results are close to the ACE-FTS measurements and the difference is usually less than 30%. In contrast, MLS shows a negative bias with a ratio as small as 0.1 at around 30 hPa and SMR shows a positive bias with a ratio as large as 4 compared to CMAM near 100 hPa.

In the upper troposphere, the largest ACE-FTS/CMAM ratio is usually close to 1.5 in the southern hemisphere for all seasons except at southern middle latitudes in the fall season, while the maximum ratios are about 2–3 in the tropics and the northern hemisphere. MLS observations show ratios as large as 3–4 at various latitudes in the upper troposphere. These differences are due to the lack of detailed tropospheric surface sources.

4 N_2O comparisons

4.1 Monthly zonal mean cross-sections

Figure 4 shows the monthly zonal mean latitude-pressure cross-sections of N_2O from CMAM, ACE-FTS, SMR, and MLS in January, April, July, and October. The distribution of N_2O from the model is quite similar to the observations in the stratosphere below 1 hPa (~50 km). The values range from over 300 ppbv in the lower stratosphere to less than 1 ppbv in the upper stratosphere. An enhancement is evident in tropics both in the model results and measurements for all seasons, reflecting the persistent upwelling throughout the year. In addition, the values of the simulation and the observations are similar except that MLS is slightly smaller in the lower tropical stratosphere. In the

sub-tropics and sub-polar regions CMAM exhibits "mixing barriers" (shown as close contours, which suggest a large gradient, of the VMRs in the sub-tropics and sub-polar regions in the winter hemisphere) (Plumb, 2002) similar to those observed by SMR, MLS and ACE-FTS in the southern hemisphere in July and October. The "mixing barrier" can also be seen in the northern sub-tropics in January in the model results and in the measurements, but it is not so evident in the northern sub-polar regions. This is because the Arctic stratospheric vortex is not as symmetric and pole-centered as the Antarctic one and we have done simple zonal averages rather than using equivalent latitudes (the latitudes that would enclose the same area as a given potential vorticity (PV) contours, e.g. Butchart and Remsberg, 1986) which would preserve the distinction between vortex and extra-vortex air. In April, Arctic N_2O is higher than in January because mid-latitude air with high N_2O mixing ratios is mixed into high latitudes during the vortex breakup. In October, however, both the model and the observations show low N_2O concentrations above ~30 hPa in the Antarctic vortex, which has not yet broken up (Manney et al., 2005b). From the summer to the fall, both the simulation and observations display N_2O decrease in the polar stratosphere, which can be attributed to the continuous photolysis during this period. After that, it increases above 5 hPa in the winter due to the meridional transport and mixing of N_2O-rich air from the middle latitudes.

The CMAM simulation shows two maxima (or rabbit's ears) above 2 hPa in April and October. These two peaks are located at middle latitudes producing a trough in the tropics. In April, the ACE, SMR and MLS also show two peaks in the sub-tropics above 5 hPa. The double-peak feature is also shown in CH_4 measurements (see Fig. 7 and Sect. 5). It is related to the SAO at the stratopause and only occurs about every other year in the measurements (not shown, and see Sect. 7 for details). In October, the multi-year averaged observations do not show such a double-peak feature. However, the feature does occur about every other year, but it is weaker than in April and is in different calendar years from the one in April (not shown).

Comparison of the observations from each instrument indicates that their distribu-

ACPD
8, 13063–13123, 2008

tions are quite similar. However, SMR and MLS measurements have positive biases relative to ACE-FTS above about 10 hPa (~32 km) at high latitudes in the fall season (in the Antarctica in April and in the Arctic in October). In addition, MLS values rarely exceed 300 ppbv in the lower stratosphere (below 50 hPa) in tropics, showing a negative bias compared to ACE and SMR (Lambert et al., 2007).

4.2 Seasonal zonal mean profiles

Figure 5 shows the seasonal zonal mean N_2O profiles between 200–1 hPa (~12–50 km) for the same latitude bands and seasons as in Fig. 2. The ratios of the measurements to CMAM results are shown in Fig. 6. In general, the observations are in good agreement while CMAM exhibits a negative bias in the upper stratosphere.

All the measurements and the model results demonstrate similar morphologies as shown in Fig. 5. The observed and simulated profiles show that the N_2O is significantly reduced from 300–320 ppbv in the upper troposphere to several ppbv in the upper stratosphere. The decrease is primarily due to the photo-dissociation with a ~10% contribution from oxidation by $O(^1D)$. Compared to ACE-FTS, SMR has a large negative bias at some latitudes below about 150 hPa, but it has no significant difference from the ACE-FTS profiles above that height, as can be seen in Fig. 5. MLS also follows the ACE-FTS and SMR results above 50 hPa (~21 km) but shows a negative bias as large as 20 ppbv at lower latitudes below 70 hPa (~18 km). The differences are consistent with the co-located comparisons shown in Lambert et al. (2007) and Strong et al. (2008). CMAM reproduces the observations well but generally underestimates the mixing ratios above 10 hPa (~32 km). The negative bias in model results is evident in the tropics throughout the seasons and in the southern hemisphere during September–November and December–January.

However, the ratios of observations to model results, illustrated in Fig. 6, show varying levels of agreement. Below 10 hPa (~32 km) the ratios are generally within 0.85 ~1.15 for most regions and seasons. At southern high latitudes for the periods December–February and September–November, the same degree of agreement

ACPD
8, 13063–13123, 2008

is only achieved at lower altitudes near 30 hPa (~25 km). Above these altitudes, the ratios increase greatly. The maxima of the ratios vary from 3 to 10 at various latitudes throughout the seasons, indicating that CMAM results are significantly smaller than the measurements, certainly outside the error of the observations. A study underway (also see Sect. 6) of eddy diffusion for tracers associated with non-orographic gravity wave drag (GWD) in CMAM suggests that an increase in vertical diffusion for chemical tracers, using the GWD scheme, would improve agreement with the measurements in the middle and upper stratosphere.

The ratios of the CMAM results averaged at the ACE-FTS observation latitudes to the means of all the CMAM results in these latitude bands, which are shown as the black dash dot lines in Fig. 6, are generally close to 1 except in the upper stratosphere at high latitudes in the winter and summer and in the tropics from March through August. This suggests that the effect of the varying ACE-FTS latitudes on the representativeness of the ACE-FTS seasonal zonal means is generally small. As for the CO ratios this effect is reduced in the ACE-FTS/CMAM ratios derived from ACE-FTS averages and CMAM averages at the ACE-FTS observation latitudes. Therefore, the ACE-FTS/CMAM ratios can also be compared to the ratios of SMR/CMAM and MLS/CMAM, which yields the differences between the ACE-FTS and the SMR and MLS retrievals.

In Fig. 6, the ratios of the SMR and MLS measurements to CMAM are generally quite similar, suggesting that SMR and MLS are in good agreement between 100–1 hPa. The ratios of ACE-FTS/CMAM near the ACE-FTS latitudes are also close to the ratios of SMR/CMAM and MLS/CMAM over most of the lower and middle latitudes, but show differences in the upper stratosphere (above 10 hPa) at high latitudes. The good agreement is consistent with the recent comparisons of co-located MLS (or SMR) and ACE-FTS observations which demonstrate their differences are generally within 10% in global average or zonal means (Lambert et al., 2007; Strong et al., 2008). However, the differences in the upper stratosphere at high latitudes show that the MLS and SMR zonal means have a positive bias with a factor of two or larger relative to ACE-FTS. The large relative difference between ACE-FTS and SMR at high altitudes in polar regions

was also reported by Strong et al. (2008).

5 CH_4 comparisons

In this section modeled and measured CH_4 profiles are compared. Unlike CO and N_2O, CH_4 is not measured by the SMR or MLS instruments and our comparison is only with ACE-FTS. The monthly zonal mean cross-sections for January, April, July and October are shown in Fig. 7, while the seasonal zonal mean profiles and the relative ratios are shown in Figs. 8 and 9, respectively.

It can be seen from Fig. 7 that CMAM CH_4 is quite similar to the ACE-FTS observations below 1 hPa (~50 km) in the stratosphere. Both the simulation and the observations show the tropical peak which is also apparent in the N_2O fields. This can be attributed to the continuous upwelling in the tropics (e.g. Plumb, 2002; Shepherd, 2007). Both model results and measurements show a decrease in the upper stratosphere in the polar regions from summer to fall due to destruction by OH. The ACE-FTS shows strong gradients in the stratosphere at 60° N in January and at 60° S in July. Individual profiles also indicate smaller CH_4 mixing ratios inside the polar vortex than outside it in January 2005 (e.g. Jin et al, 2006). The CMAM also shows CH_4 decrease in the lower stratosphere from fall to winter because of the descent of mesospheric air with low mixing ratios of CH_4 inside the winter polar vortex. The CMAM CH_4 shows mixing barriers similar to those revealed by N_2O in the sub-tropics and sub-polar regions in the winter hemisphere. The simulated values are also close to the observations below about 1 hPa except that CMAM is ~0.1 ppmv larger than the ACE-FTS near the tropical tropopause. Above 1 hPa, however, CMAM is generally smaller except at southern high latitudes in January.

Below 1 hPa, Figs. 8 and 9 show that the seasonal mean profiles are similar and the ratios of the ACE-FTS observations to the CMAM simulation at the ACE-FTS latitudes are mostly within 0.85–1.15. One exception is that the ratio is about 1.5–2 near 5 hPa (~37 km) in the southern middle and high latitudes, indicating smaller model val-

ues. At high latitudes this is probably related to the descent of air with a low CH_4 bias from above (see the following discussion). Above 1 hPa, although the absolute difference between the simulated and observed mixing ratio profiles is generally less than 0.2 ppmv, the ratios of ACE-FTS/CMAM depart significantly from the value 1.0. The maxima of the ratios range from 1.5–7, showing a low bias in the CMAM simulation.

This low bias suggests that the transport from the lower stratosphere to the upper stratosphere in the model is slower than in the atmosphere thus allowing for more chemical destruction. Previous comparisons of CMAM CH_4 with HALOE observations (Russell et al., 1993a) also showed a good agreement below 1 hPa (Zhang, 2002; Eyring et al., 2006). Figure 9 also shows the ratios of ACE-FTS N_2O observations to the CMAM N_2O simulation at the ACE-FTS latitudes. Although the ratios for N_2O are in general significantly larger than the ratios for CH_4, their departures from the value 1.0 occur at similar altitudes. Since the chemical destruction processes of CH_4 and N_2O are different, this pattern strongly suggests the negative biases are due to model transport behavior in the upper stratosphere.

The difference between the ratios for N_2O and CH_4 above 10 hPa can perhaps be attributed to the treatment of vertical diffusion in the standard CMAM model. In the appendix, for a species whose profile is determined by chemical loss and supply by transport, we show that its scale height is determined by a ratio connecting the chemical lifetime and the vertical diffusion. The scale height for a shorter-lived species is smaller than a relatively longer-lived species, and thus the mixing ratios of a short-lived species decrease more quickly than the relatively longer-lived species. In other words, if the diffusion is smaller in a model than in the atmosphere, the model results would have a larger negative bias for a relatively shorter-lived species than a relatively longer-lived species which is the case for N_2O versus CH_4. We note that in the CMAM version used this study, the only vertical diffusion in the stratosphere and lower mesosphere is due to wind shear with mean $K_z \leq 0.6\,m^2s^{-1}$ and due to a background eddy diffusion of $0.1\,m^2s^{-1}$. As a result, the modeled N_2O and CH_4 not only are smaller than the measurements, but also differ in their negative biases. The local chemical lifetimes

ACPD
8, 13063–13123, 2008

of N_2O and CH_4 are about a few weeks and a few months, respectively, in the upper stratosphere. Therefore, the simulated N_2O has a relatively larger negative bias than the simulated CH_4. Furthermore, our ongoing study shows that the behavior of N_2O and CH_4 can be improved by introducing the diffusion associated with the GWD in the stratosphere and lower mesosphere (paper in preparation).

6 Polar descent

Measurements of long lived species such as CO, CH_4, N_2O and H_2O indicate that polar mesospheric air can be transported downward into the stratosphere with a limited degree of dilution (Schoeberl et al., 1992, 1995; Manney et al., 1995; Abrams et al., 1996a and b; Allen et al., 1999, 2000; Manney et al., 2007; Juckes, 2007) and this is also seen in transport calculations (e.g., Manney et al., 1994; Plumb et al., 2002). This phenomenon is related to the rapid and deep descent inside the polar vortex from late fall to early spring. Enhanced NO_x has also been observed recently in the upper stratosphere in the Arctic in early year 2004 and 2006 (Rinsland et al., 2005, Randall et al., 2006; Hauchecorne et al., 2007; Semeniuk et al., 2008). These transport events of high concentration of NO_x occurred in the wake of major and persistent sudden stratospheric warmings (SSWs) (Manney et al., 2005a, 2008a, 2008b; Siskind et al., 2007).

The development of major SSWs involves the reversal of stratospheric zonal winds from westerly to easterly in the middle stratosphere. In the mesosphere, as a result, the non-orographic gravity wave drag changes from easterly to westerly and a westerly vortex develops (e.g. Holton, 1982). As the westerlies restore themselves in the stratosphere, the easterly gravity wave drag is restored as well in the mesosphere which enhances downward descent. A strong radiative cooling in the upper stratosphere and lower mesosphere after SSW also leads to a strong upper-level vortex and enhances the descent (Siskind et al., 2007; Manney et al., 2008b). This enhanced descent creates a window for relatively confined transport of NO_x from the mesopause region in

the polar night (Semeniuk et al., 2008).

The CO measurements along with other tracers such as H_2O from ACE-FTS and MLS showed an evident enhancement in the Arctic upper stratosphere after a strong SSW during the winters 2004 and 2006, and showed a strong enhancement in the Arctic middle stratosphere inside a strong stratospheric vortex during the winter 2005 (Randall et al., 2006; Manney et al., 2007, 2008a). The change of the zonal wind during SSWs was observed at Poker Flats, Alaska (65° N, 147° W) during the Arctic winters 2002 and 2004 (Jones et al., 2007). A detailed description of the evolution of the Arctic SSWs during the winters 2004 and 2006 is offered by Manney et al. (2005a) and Manney et al. (2008b), respectively, based on satellite observations and assimilated meteorological analyses. In this section, we compare time-altitude slices of the polar descent in stratosphere and mesosphere from CMAM with recent CO measurements from MLS, ACE-FTS and SMR.

A full picture of observed annual evolution of CO in the polar stratospheric and mesospheric is lacking although previous measurements and simulations revealed its strong seasonal variability in the middle atmosphere (Clancy et al., 1984; Solomon et al., 1985). Several long term ground based measurements were reported recently (Forkman et al., 2003, 2005; Velazco et al., 2007), which have improved the understanding of seasonal variability in the Arctic. However, these observations either have low vertical resolution or lack information on the stratospheric evolution. Consecutive CO measurements with high vertical resolution and global coverage have been conducted by satellite instruments ISAMS on UARS (López-Valverde et al., 1996; Allen et al., 1999, 2000), SMR on Odin (Dupuy et al., 2004), ACE-FTS (Clerbaux et al., 2005) and MLS on Aura (Pumphrey et al., 2007). Seasonal variability has been shown in these studies, but the annual evolution of the CO distribution in the stratosphere and mesosphere in the Arctic and the Antarctica has not yet been described. In this section, we also provide measurements in the Arctic during periods 1 July 2004–1 July 2005, and 1 July 2005–1 July 2006 and average observations in the Antarctica during the past three years 2004–2007, and compare them to CMAM results.

Panel A in Figs. 10 and 11 shows the MLS CO measurements near the North Pole (70° N–82° N) during periods of 1 July 2004–1 July 2005 and 1 July 2005–1 July 2006. Because the model results are from a climatological simulation, exact reproduction of the observations in each calendar year is not expected. So we choose the CMAM simulation in two periods of 1 July 2006–1 July 2007 and 1 July 2004–1 July 2005 when minor and strong Arctic SSWs occurs as indicated by the CO evolution (see panel C in Figs. 10 and 11). In addition, the daily zonal mean of ACE-FTS CO observations north of 50°N for the periods of 1 July 2004–1 July 2005 and 1 July 2005–1 July 2006 are shown in panel B in Figs. 10 and 11, while the CMAM zonal means near the ACE-FTS latitudes for the model periods of 1 July 2006–1 July 2007 and 1 July 2004–1 July 2005 are shown in panel D in Figs. 10 and 11.

The winter of 2004/2005 was identified as one of the coldest winters ever observed in the Arctic stratosphere and there was a strong stratospheric polar vortex before its early breakup in March 2005 (Manney et al., 2006, 2008a). As a result, significantly increased CO mixing ratios can be seen in the stratosphere during the winter season (November 2004–March 2005) (see Fig. 10 panels A and B). Air containing 0.1 ppmv CO, located in the lower mesosphere at around 0.1 hPa (~65 km) in late September 2004, descended to 20 hPa (~28 km) in some locations by mid-March 2005, reflecting rapid downward transport in the polar region: of course there is no CO production and its loss is extremely slow during the polar night. In mid-March 2005, the stratospheric vortex broke up and the high CO mixing ratio air was quickly diluted with low CO mixing ratio air from mid-latitudes. The Arctic stratosphere CO evolution during the winters of 2004/2005 and 2005/2006 is also shown by Manney et al. (2007, 2008a). In the winter mesosphere, where the lifetime of CO is very long, the CO concentration stabilized above around 0.1 hPa (~65 km) after the rapid increase in September–October, and the CO enriched air was not diluted until April/May 2005. The rapid increase in Fall and decrease in Spring are related to the onset of descent and ascent resulting from the mesospheric pole-to-pole meridional circulation (Plumb, 2002; Shepherd, 2007). The flatness of the CO isopleths in the winter mesosphere indicates that an equilibrium

between vertical transport and horizontal mixing is established quickly and maintained.

The CMAM simulation shown in panel C in Fig. 10 has a very similar morphology to the MLS measurements. There is similar descent of CO rich air from the mesosphere into the lower stratosphere from fall to spring and CO decrease in later spring. However, there is a significant reduction of CO in the middle and upper stratosphere after mid-January, which is due to a SSW and the associated mixing with mid-latitude low CO mixing ratio air. This is more clearly seen in measurements and simulations with strong SSWs as discussed below. The CMAM results also follow ACE-FTS measurements (see panels B and D) very well over the Arctic regions throughout the year. Around 1 March, however, CMAM is larger than ACE-FTS above 10 hPa. In fact, CMAM is also larger than the MLS above 10 hPa near the North Pole around 1 March. This difference can be attributed to the strong vortex in the selected model period and the early breakup of the Arctic stratospheric vortex in March 2005 although it was very strong in January and February 2005 (Manney et al., 2007, 2008a).

Panel A in Fig. 11 shows the Arctic CO evolution observed by MLS in winter 2005/2006 when a strong and long-lasting SSW occurred in early January 2006 (Manney et al., 2008b). As a result, the high CO air was rapidly diluted in mid-January below 0.1 hPa (~65 km). However, the mesospheric air above was not disturbed until late January 2006. Previous studies have shown that the stratopause broke down in late January, then reformed at about 0.01 hPa (~75 km) and a cold upper stratospheric vortex formed below it (Siskind et al., 2007; Manney et al., 2008b). After that, the air isolated in this recovered vortex started to descend above 0.5 hPa, and the downward tongue, which is a distinct feature from the winter 2004/2005, is seen in the upper stratosphere and lower mesosphere (above 2 hPa) in the spring. The CO concentration is even larger than that before the SSW. This CO downward tongue is also observed by ACE-FTS (see panel B, also shown by Randall et al., 2006).

Panel C in Fig. 11 shows CMAM Arctic simulations with a major SSW in January and two minor SSWs in November and March. The major SSW that happened to develop in one of the four model years is not as strong as seen in the observations so that CO is

ACPD
8, 13063–13123, 2008

not diluted to pre-vortex background values (compare with panels A and B). However, the evolution of the model temperature (not shown) does exhibit similar features compared with the observations (Manney et al., 2008b): the temperature decreases over 20 K, which suggests there is a strong radiative cooling and enhanced descent, in the upper stratosphere and lower mesosphere after the SSW. In addition, the mesospheric CO is immediately disturbed by the SSW in the simulation. Nevertheless, the descent from the mesosphere into the stratosphere after the SSW (although the CO mixing ratio is not larger than that before the SSW as is the case in the observations) agrees with the observations of downward transport following a strong SSW in mid-winter. We also note that there is a CO disturbance in the upper stratosphere in November and March in model results. CMAM zonal means near the ACE-FTS latitudes are shown in panel D. Although the CMAM model results at the northern high latitudes show the CO enhancement after the major SSW (panel C), CMAM results sampled near the ACE-FTS locations do not display this feature, which suggests that the restored upper-level vortex is too small and short-lived. However, we note that the difference does not necessarily point to a deficiency in the model since the simulated SSW is modeled in a climate model and is not expected to match exactly the strong SSW during the winter 2006. Obviously, further investigation of the characteristics of the model's SSW behavior is needed.

In order to further demonstrate the downward transport from the mesosphere into the stratosphere after SSWs, pressure-latitude cross-sections of SMR CO measurements between November 2003–March 2004 along with MLS CO cross-sections between November 2004–March 2005 and November 2005–March 2006 are shown in Fig. 12. The Arctic winter 2004 was also exceptional for a strong SSW that started in late December 2003 persisted through January 2004 and the subsequent reformation of a strong and cold upper stratospheric vortex (Manney et al., 2005a). Since CMAM is a climatological model, the simulation cannot match the observations on specific days. Therefore, the model results are not shown in Fig. 12 for comparison. The CO mixing ratio in later November and early December 2003 is smaller than in the subsequent

years 2004 and 2005. During the sudden warming, the CO mixing ratio was reduced in the stratosphere in late December 2003, resulting in significantly smaller CO concentrations in the stratosphere compared to those measured during the same period in the winters 2005 and 2006. However, there was also a significant increase above ~0.5 hPa at the end of January 2004 and in the middle of February 2004. The CO enhancement was due to the enhanced descent inside the re-formed cold upper stratospheric vortex. In 2005, however, the air with large CO mixing ratios descended as low as 5 hPa–10 hPa in January and February before being mixed with middle latitude low CO mixing ratio air in March. This reflects descent inside the strong stratospheric polar vortex and its break-up as discussed above. The cross-sections in 2006 also show consistency with the evolution shown in Fig. 11, panel A, in that polar stratospheric CO has been diluted by the end of January while downward transport in the upper stratosphere and lower mesosphere (above 0.5 hPa) can be seen during 15–16 February 2006 and 22–23 March 2006.

The figure also clearly shows the similarities in the CO distributions in 2004 and in 2006: no elevated CO is confined in the lower and middle stratosphere in northern high latitudes in late winter and early spring, while enhanced CO can be seen in the upper stratosphere and lower mesosphere. In addition, more CO is seen below 0.1 hPa (~65 km) on 29–30 January 2004 than on 29–30 January 2006 at high latitudes. This suggests that the upper stratospheric vortex was stronger in late January 2004 than in late January 2006, which is consistent with previous analyses that the SSW and the upper stratospheric vortex occurred slightly earlier in 2004 than in 2006 (Manney et al., 2005a, 2008a). The ACE-FTS observations also show the enhanced CO concentration in the upper stratosphere in February–March 2004 and 2006 compared to the winter 2005 (see Fig. 1 in Randall et al. (2006)). In short, the CO measurements in these three winters show that there was an enhanced descent in the upper stratosphere following a prolonged SSW after which the upper stratospheric vortex redeveloped very strongly.

Figure 13 shows the multi-year averaged CO in the Antarctica from MLS (panel A), ACE-FTS (panel C) and CMAM (panels B and D). They all demonstrate very similar

ACPD
8, 13063–13123, 2008

annual CO evolutions throughout the domain. However, CMAM mixing ratios are evidently larger than MLS values in the mesosphere from April to October. The modeled air with 1 ppmv CO at high southern latitudes is found at lower altitudes (about 2 hPa) than in the MLS measurements (about 0.5 hPa) in July. Furthermore, the CO tongue, which reflects the residual stratospheric vortex at high latitudes in late spring, did not vanish until late November in the model results (panel B), while it disappeared at the beginning of November in the MLS measurements. The CO distributions of ACE-FTS and CMAM are generally very similar throughout the year. The tongue shown by MLS and CMAM in panels A and C does not extend into the lower stratosphere in ACE-FTS and CMAM sampled near ACE latitudes because of the absence of ACE-FTS observations at high latitudes in October. However, CMAM does shows a maximum at 20–10 hPa in November while it is not evident in ACE-FTS measurements. All these differences suggest that CMAM has a later break-up of the Antarctic polar vortex than the real atmosphere (Shepherd, 2000; Eyring et al., 2006) as discussed in Sect. 3.

An inter-hemispheric comparison shows a similar mesospheric CO morphology above about 0.1 hPa (~65 km) in the Antarctica as in the Arctic in the absence of a major SSW. However, there is a prolonged stratospheric CO enhancement in the Antarctica in spring, because the stratospheric vortex in the Antarctica is generally stronger and longer lasting than in the Arctic.

7 Comparisons of tropical oscillations

In the tropics, convection and land-sea surface contrasts drive major wave activity which propagates into the middle atmosphere (e.g. Baldwin et al., 2001 and references therein). This wave activity can leave its signature on the distribution of minor species. For example, the water vapour and CO "tape recorders" (e.g. Mote et al., 1996; Randel et al., 2004; Schoeberl et al., 2006) in the upper troposphere and lower stratosphere (UT/LS), the quasi-biennial oscillation (QBO) and the semi-annual oscillation (SAO) in ozone and water vapour in the stratosphere and mesosphere (e.g. Ray et al., 1994;

Randel and Wu, 1996; Garcia et al., 1997; Dunkerton, 2001; Tian et al., 2006; Huang et al., 2008). Schoeberl et al. (2006) suggested that part of the CO tape recorder signal (or annual oscillation, in the lower stratosphere) is due to seasonal changes of surface sources such as biomass burning. Thus the behavior of this signal is superimposed on the dynamical signature. Other studies have shown that the signal is driven by the tropical upwelling due to annual temperature oscillation (Randel et al., 2007) and by the Brewer-Dobson circulation (Schoeberl et al., 2008) in the lower stratosphere. The SAO and QBO in the chemical tracers are also determined by the wind and temperature oscillations associated with the middle atmospheric circulation (e.g. Gray and Pyle, 1986; Ray et al., 1994; Baldwin et al., 2001).

In this section, we qualitatively compare the signals in the CMAM simulation with those in the satellite observations. We note that ACE-FTS observations are not used in this section. Because the prime objectives for SCISAT-1 were focused on polar regions the orbit design yielded limited coverage of the tropics, although careful employment of them did produce valuable information on seasonal convective outflow at the tropical tropopause (Folkins et al., 2006) and the tropical tape recorder of HCN (Pumphrey et al, 2008). The anomalies of the zonal mean CO, CH_4 and N_2O over their annual averages are shown in Figs. 14, 15 and 16.

First, the CMAM results show a morphology similar to the observed CO tape recorder in the lower stratosphere. In Fig. 14, panels A, B and C, MLS CO observations demonstrate a seasonal variation below 50 hPa (20 km), which was identified as a tape recorder-like signal linked to the seasonal change of biomass burning by Schoeberl et al. (2006). In panels D, E and F, the seasonal variation of CMAM CO is evident between 100–50 hPa (16–20 km). The +1 ppbv positive anomaly and –1 ppbv negative anomaly start from December and July, respectively. The maximum and the minimum values of the anomalies are about +3 ppbv and –3 ppbv, respectively. As noted above there are no biomass burning sources in the simulation, therefore the oscillation reveals a purely dynamical signal. Its amplitude is thus expected to be smaller than in the observations. As a result, the upper tropospheric (below 150 hPa) CO enhancement is not

seen in the model. Aside from these differences, the oscillation in the model shows a similar temporal evolution of the upward motion in the lower stratosphere. Since the upper tropospheric variation is not significant, the model variation suggests that diabatic upwelling and the Brewer-Dobson circulation are reasonably well characterized in the model. There are also similar seasonal variations of CH_4 and N_2O between 100–20 hPa (16–28 km) in the model results (Fig. 15, panels A and B, and Fig. 16, panels C and F). A similar seasonal variation of N_2O can be seen in the SMR measurements although their amplitude is larger in the model (Fig. 16, panels A and D). The highly positively correlated N_2O and CH_4 oscillations in the model results confirm that the variations are due to transport. However, between 100–20 hPa there is a vertical displacement between the N_2O and CH_4 oscillations and the variations of CO, the latter of which are only evident between 100–50 hPa, although they all show similar temporal evolution. This difference is likely simply due to the shorter chemical lifetime of CO transported in the UT/LS as compared to the much longer lifetimes of both N_2O and CH_4.

Figure 14 shows another feature common in the observations and model: The SAO of tracer concentrations at the mesopause and stratopause. Two large CO positive anomalies occur above 0.005 hPa (~85 km) in April–May and October–November in both CMAM and MLS, suggesting presence of a significant SAO signal at the mesopause. The one occurring in the first half of the calendar year stays at the mesopause and decreases quickly to a negative anomaly in June. However, the one in the second half of the calendar year descends during the subsequent months and reaches the stratopause (about 1 hPa) in February–March when it merges with one of the positive anomalies at the stratopause. At the stratopause, CMAM exhibits another positive anomaly in September–October. Descent of the positive and negative anomalies originating at the stratopause in the first half of the calendar year (and subsequent months too) can be seen above about 10 hPa (32 km). However, the anomalies originating at the stratopause in the second half of the year stay above ~3 hPa (40 km). The MLS CO measurements exhibit similar semi-annual oscillations in the middle and

upper stratosphere (panels A and B). There is also a clear downward propagation of the first pair of anomalies while it is not evident for the second pair.

The SAO in the CO field is in phase with the oscillations of model temperature (not shown) and observed temperature (Garcia et al., 1997): the positive anomaly of CO is associated with the warm anomaly in the temperature field. The positive anomaly is also associated with the observed westerly wind shear (Hirota, 1978; Garcia et al., 1997). When considering that CO increases with height in the mesosphere, we may conclude that the positive anomaly of CO is driven by the descent associated with a secondary meridional circulation during the westerly phase of the oscillation (Andrews et al., 1987). In addition, the SAO in MLS and CMAM CO field is in phase with the SAO in the SABER (Sounding of the Atmosphere using Broadband Emission Radiometry) O_3 field above 0.01 hPa (~80 km) (Huang et al., 2008). This is not surprising since O_3 also increases with height due to the local chemical production in the tropical mesosphere. However, the CO field shows a strong annual oscillation between 0.5–0.05 hPa (53–70 km), while the SABER O_3 field shows the SAO. The reason for this difference is not clear at the moment.

The SMR and MLS N_2O measurements also show an SAO signature at the stratopause (Fig. 16). We find that the CMAM N_2O oscillations are in general agreement with the SMR and MLS measurements but with a smaller amplitude except for the spatially larger anomaly at 2 hPa in September. Both measurements and model results show that the first cycle in the calendar year is stronger than the second, which is consistentwith previous reports, e.g. SAO in ozone observations (Ray et al., 1994). The SAO is also evident in the CMAM CH_4 field (Fig. 15), and the maximum amplitude of the CH_4 anomalies exceeds 100 ppbv at the stratopause. In addition, the SAO in CMAM stratospheric N_2O and CH_4 fields are locked in phase, which is not surprising since N_2O and CH_4 are similar long-lived tracers in the stratosphere and both are emitted from the Earth's surface.

The similarity of the SAO signal in the both observed and simulated N_2O fields suggests that the model is capturing important dynamical features. The temperature SAO

ACPD
8, 13063–13123, 2008

at the stratopause in CMAM (not shown) is also in good agreement with the SABER observations reported by Huang et al. (2008). Comparisons of the zonal wind SAO at the stratopause in CMAM (Medvedev and Klaassen, 2001) and observations (Hirota, 1978, Garcia et al., 1997) indicate that the positive anomalies in these tracers are associated with easterly wind shear and negative temperature anomalies while the negative anomalies in the tracers are associated with westerly wind shear and positive temperature anomalies. This is also consistent with the understanding of the SAO in long-lived tracers (e.g. Gray and Pyle, 1986; Ray et al., 1994).

The anomalies in the CO field are also in phase with the anomalies of N_2O and CH_4 at the stratopause. When considering that CO is produced from CH_4 in the stratosphere, we can attribute the SAO of CO to the oscillations of CH_4.

In addition, the inter-annual variation of the SAO in SMR N_2O field shows a biennial oscillation. The SMR N_2O anomalies over a long term (July 2001–February 2007) mean are shown in Fig. 16, panel D. It can be seen that that the large positive anomalies in the SAO cycles propagate downward in the upper stratosphere and the temporal interval between the propagation is about two years. Comparing with the QBO of the zonal wind given in Schoeberl et al. (2008) it is found that the QBO is in its westerly phase (the wind is westerly at 40 hPa) during the years 2002, 2004 and 2006 when the first positive N_2O anomaly in the calendar year occurs at relative higher altitudes, while the QBO is in its easterly phase during the years 2003 and 2005 when the first positive anomaly in the calendar years occurs at relative lower altitudes. The latter condition corresponds to the prominent double-peak in N_2O at the extra-tropical stratopause, which is displayed in the panel for April in Fig. 4. (However, we recall that Fig. 4 shows multi-year averages). When the QBO is in its westerly phase, the double-peak feature is barely discernible. A relation of the SAO and QBO was also demonstrated by HALOE CH_4 measurements by Ruth et al. (1997) and Randel et al. (1998) and summarized by Baldwin et al. (1999). However, in their reports the prominent double-peak feature occurred in April 1993 and 1995 during the westerly QBO phase, which is different from the recent measurements. Thus the combination of the previous and current reports

suggests that the relationship between the inter-annual variation of SAO in tracer fields and the QBO of the zonal wind is not well-understood (Baldwin et al., 2001) and that the double-peak feature and the SAO may have a biennial oscillation instead of the quasi-biennial oscillation. Obviously, a more comprehensive analysis of the SAO-QBO link is outside the scope of this paper. The inter-annual variation of the SAO in the MLS N_2O field also shows a biennial oscillation. In addition, the variation is very similar with that in the SMR N_2O field during the overlap period August 2004–January 2007. Details about the phase and amplitude of the MLS N_2O SAO and QBO can be found in Schoeberl et al. (2008). The CMAM N_2O anomalies over 4-year mean are shown in Fig. 16, panel F. Since the version of the model used in this study does not capture the dynamical QBO, it is not surprising to see that the SAO in the model results fails to follow the inter-annual variation shown by the measurements.

8 Summary

In order to further evaluate the chemistry climate model CMAM, the model results of CO, N_2O and CH_4 for model year 2004–2007 have been compared with the recent measurements from the satellite instruments Odin/SMR, ACE-FTS, and Aura/MLS. The comparison shows that CMAM reproduces the main characteristics of the CO distribution and temporal evolution very well. The differences between the model and the measurements are generally less than 30% in the middle atmosphere. The difference is comparable with the difference between the instruments (see also Pumphrey et al., 2007). Above the middle stratosphere (10 hPa), the CO measurements show a good agreement between ACE-FTS, MLS and SMR although MLS usually shows a positive bias compared to ACE-FTS while SMR has a negative bias. However, at about 30 hPa, MLS shows a large negative bias compared to CMAM and the other two instruments, especially in the tropics. In the lower stratosphere and troposphere, CMAM CO values are smaller than the measurements because of the absence of realistic surface emissions in the model. However, differences between measurements are also

ACPD
8, 13063–13123, 2008

large, suggesting that improvements in the measurements and/or retrieved values in this region are needed.

CMAM also reproduces the seasonal CO variation at high latitudes very well. All the measurements and the model results show the strong meridional increase towards the winter polar regions, which is due to the meridional transport in the mesosphere and descent into the stratospheric polar vortex. The complete annual evolution of CO in the Arctic and Antarctica is also presented in this study. Both the observations and simulation show that mesospheric air can descend into stratosphere as low as 20 hPa in both the Arctic and Antarctic. However, in the Antarctica the large CO concentrations in the lower stratosphere in November indicate that the CMAM polar vortex is too persistent. In addition, the SMR and MLS CO measurements demonstrate strong descent in the recovery phase of the upper stratospheric Arctic polar vortex following the SSWs in the winters of 2004 and 2006. CMAM also shows this rapid descent in the upper stratospheric polar vortex in the wake of a SSW. However, CMAM sampled at the ACE-FTS latitudes does not show this feature, which is also shown by ACE-FTS. Nevertheless, we note that the comparison here is between a climatological simulation and observations in a particular year and thus the difference does not necessary mean there is a deficiency in the model although further investigation of the model's behavior during and after SSWs is needed.

CMAM simulates lower and middle stratospheric N_2O and CH_4 very well. The model-measurement comparison, however, has highlighted the need for improvement of the vertical sub-grid scale diffusion in CMAM. In general, the "mixing barriers" which is evident in the CMAM monthly mean cross-sections are quite realistic. The CMAM results are generally within 15% of the N_2O and CH_4 measurements. Apart from the fact that the MLS N_2O has a low bias of about 20 ppbv in the lower tropical stratosphere and that MLS and SMR have high biases in the polar upper stratosphere compared to ACE-FTS, the N_2O measurements from these three instruments demonstrate excellent agreement in the stratosphere.

CMAM captures the tropical tape recorder (or annual oscillation) and SAO. The ab-

ACPD
8, 13063–13123, 2008

sence of biomass and fossil fuel burning emissions in the model simulation allows for a clear signature of the annual variation of tropical upwelling in the CO. The CO tape recorder indicates CMAM has a reasonable upward motion in the tropical lower stratosphere. Despite that the modeled amplitude of the SAO is smaller and the biennial variation of the SAO shown by the SMR and MLS observations is not reproduced by the model, the SAO in CMAM generally shows good agreement with the observations.

Appendix A

Scale height for species

When considering a simple one-dimension model, the vertical flux, φ_i, of a species "i" of volume mixing ratio f_i is given by

$$\varphi_i = -K_Z M \frac{df_i}{dz} \tag{A1}$$

where K_Z is the vertical eddy diffusion coefficient and is, for simplicity, assumed to be a constant although it varies with atmospheric conditions and chemical species (Andrews et al., 1987). M is the total air number density. If the species has no local chemical source but only a loss process of frequency L_i, the continuity equation can be written in steady state

$$\frac{d\varphi_i}{dz} = -L_i f_i M \tag{A2}$$

Combining these into a single equation and assuming that the atmosphere is isothermal with scale height, H_{av}, we obtain

$$\frac{d^2 f_i}{dz^2} - \frac{1}{H_{av}} \frac{df_i}{dz} - \frac{L_i}{K_Z} f_i = 0 \tag{A3}$$

If we assume that $f_i = f_{i0} \exp(-\alpha_i z)$, then substituting it into (A3), we find that α_i satisfies

$$\alpha_i^2 + \frac{1}{H_{av}}\alpha_i - \frac{L_i}{K_Z} = 0 \tag{A4}$$

or α_i is given by

$$\alpha_i = -\frac{1}{2H_{av}} \pm \sqrt{\frac{1}{(2H_{av})^2} + \frac{L_i}{K_Z}} = -\frac{1}{2H_{av}} \pm \frac{1}{2H_{av}}\sqrt{1 + \frac{4H_{av}^2 L_i}{K_Z}} \tag{A5}$$

The role of the chemical lifetime is made more explicit if we look at limiting cases when the second term under the square root is both >1 and <1 which will occur for short-lived and long-lived species (short and long-lived in the context of a given K_Z). For the first case ("short-lived" species) which for $K_Z \sim 1\mathrm{m}^2\mathrm{s}^{-1}$, $H_{av} \sim 7\,\mathrm{km}$ then $L_i > 10^{-7}\mathrm{s}^{-1}$ or a local chemical time constant <3 months. In this case, neglecting the first term on the right hand side we obtain $\alpha_i = \sqrt{L_i/K_Z}\,\mathrm{m}^{-1}$ or the scale height of the minor species mixing ratio,

$$H_i = 1/\alpha_i = \sqrt{K_Z/L_i}\,\mathrm{m} \tag{A6}$$

For long-lived species expanding the term under the square root sign and choosing the + root we obtain

$$\alpha_i \approx +\frac{H_{av} L_i}{K_Z} \tag{A7}$$

In each case the role played by the chemical lifetime, $\tau_{\mathrm{chem}} = 1/L_i$, is evident.

Acknowledgements. The authors would like to thank the Canadian Space Agency (CSA), the Natural Sciences and Engineering Research Council (NSERC) of Canada and the Canadian Foundation for Climate and Atmospheric Science for support. Computing resources were also provided by the Canadian Foundation for Innovation and the Ontario Innovation Trust. Work

at the Jet Propulsion Laboratory, California Institute of Technology was done under contract with the National Aeronautics and Space Administration. Odin is a Swedish-led satellite project funded jointly by the Swedish National Space Board (SNSB), the CSA, the Centre National d'Études Spatiales (CNES) in France and the National Technology Agency of Finland (Tekes).

References

Abrams, M. C., Manney, G. L., Gunson, M. R., Abbas, M. M., Chang, A. Y., Goldman, A., Irion, F. W., Michelsen, H. A., Newchurch, M. J., Rinsland, C. P., Salawitch, R. J., Stiller, G. P., and Zander, R.: Observations of Long-Lived Tracers and Descent in the Antarctic Vortex in November 1994, Geophys. Res. Lett., 23(17), 2341–2344, 1996a.

Abrams, M. C., Manney, G. L., Gunson, M. R., Abbas, M. M., Chang, A. Y., Goldman, A., Irion, F. W., Michelsen, H. A., Newchurch, M. J., Rinsland, C. P., Salawitch, R. J., Stiller, G. P., and Zander, R.: Trace Gas Transport in the Arctic Vortex Inferred From ATMOS ATLAS-2 Observations During April 1993, Geophys. Res. Lett., 23(17), 2345–2348, 1996b.

Allen, D. R., Stanford, J. L., López-Valverde, M. A., Nakamura, N., Lary, D. J., Douglass, A. R., Cerniglia, M. C., Remedios, J. J., and Taylor, F. W.: Observations of middle atmosphere CO from the UARS ISAMS during the early northern winter 1991/1992, J. Atmos. Sci., 56, 563–583, 1999.

Allen, D. R., Stanford, J. L., Nakamura, N., López-Valverde, M. A., López-Puertas, M., Taylor, F. W., and Remedios, J. J.: Antarctic polar descent and planetary wave activity observed in ISAMS CO from April to July 1992, Geophys. Res. Lett., 27(5), 665–668, 2000.

Andrews, D. G., Holton, J. R., and Leovy, C. B.: Middle Atmospheric Dynamics, Academic Press, 1–489, 1987.

Austin, J., Shindell, D., Beagley, S. R., Brühl, C., Dameris, M., Manzini, E., Nagashima, T., Newman, P., Pawson, S., Pitari, G., Rozanov, E., Schnadt, C., and Shepherd, T. G.: Uncertainties and assessments of chemistry-climate models of the stratosphere, Atmos. Chem. Phys., 3, 1–27, 2003, http://www.atmos-chem-phys.net/3/1/2003/.

Baldwin, M. P., Gray, L. J., Dunkerton, T. J., Hamilton, K., Haynes, P. H., Randel, W. J., Holton, J. R., Alexander, M. J., Hirota, I., Horinouchi, T., Jones, D. B. A., Kinnersley, J. S., Marquardt,

C., Sato, K., and Takahashi, M.: The Quasi-Biennial Oscillation, Rev. Geophys., 39(2), 179–229, 2001.
Barret, B., Ricaud, P., Santee, M. L., Attié, J.-L., Urban, J., Le Flochmoën, E., Berthet, G., Murtagh, D., Eriksson, P., Jones, A., De La Noë, J., Dupuy, E., Froidevaux, L., Livesey, N. J., Waters, J. W., and Filipiak, M. J.: Intercomparisons of trace gases profiles from the Odin/SMR and Aura/MLS limb sounders, J. Geophys. Res., 111, D21302, doi:10.1029/2006JD007305, 2006.
Beagley, S. R., de Grandpré, J., Koshyk, J. N., McFarlane, N. A., and Shepherd, T. G.: Radiative-dynamical climatology of the first-generation Canadian Middle Atmosphere Model, Atmos. Ocean, 35(3), 293–331, 1997.
Bernath, P. F.: Atmospheric Chemistry Experiment (ACE): Analytical Chemistry from Orbit, Trends in Analytical Chemistry, 25(7), 647–654, 2006.
Bernath, P. F., McElroy, C. T., Abrahams, M. C. et al.: Atmospheric Chemistry Experiment (ACE): Mission overview, Geophys. Res. Lett., 32, L15S01, doi:10.1029/2005GL022386, 2005.
Boone, C. D., Nassar, R., Walker, K. A., Rochon, Y., McLeod, S. D., Rinsland, C. P., and Bernath, P. F.: Retrievals for the atmospheric chemistry experiment Fourier-transform spectrometer, Appl. Opt., 44(33), 7218–7231, 2005.
Brasseur G. P. and Solomon, S.: Aeronomy of the middle atmosphere, 3rd ed., Springer, 2005.
Butchart, N. and Remsberg, E. E.: The area of the stratospheric polar vortex as a diagnostic for tracer transport on an isentropic surface, J. Atmos. Sci., 43, 1319–1339, 1986.
Clancy, R. T., Muhleman, D. O., and Allen, M.: Seasonal variability of CO in the terrestrial mesosphere, J. Geophys. Res., 89(D6), 9673–9676, 1984.
Clerbaux C., Coheur, P.-F., Hurtmans, Barret, B., Carleer, M., Colin, R., Semeniuk, K., McConnell, J. C., Boone, C., Bernath P. F.: Carbon monoxide distribution from the ACE-FTS solar occultation measurements, Geophys. Res. Lett., 32, L16S01, doi:10.1029/2005GL022394, 2005.
Clerbaux, C., George, M., Turquety, S., Walker, K. A., et al.: CO measurements from the ACE-FTS satellite instrument: data analysis and validation using ground-based, airborne and spaceborne observations, Atmos. Chem. Phys., 8, 2569–2594, 2008, http://www.atmos-chem-phys.net/8/2569/2008/.
de Grandpré, J., Beagley, S. R., Fomichev, V. I., Griffioen, E., McConnell, J. C., Medvedev, A. S., and Shepherd, T. G.: Ozone climatology using interactive chemistry: Results from

the Canadian Middle Atmosphere Model, J. Geophys. Res., 105(D21), 26 475–26 492, doi:10.1029/2000JD900427, 2000.
De Mazière, M., Vigouroux, C., Bernath, P. F., et al.: Validation of ACE-FTS v2.2 methane profiles from the upper troposphere to lower mesosphere, Atmos. Chem. Phys., 8, 2421–2435, 2008, http://www.atmos-chem-phys.net/8/2421/2008/.
Dunkerton, T. J.: Quasi-Biennial and Subbiennial Variations of Stratospheric Trace Constituents Derived from HALOE Observations, J. Atmos. Sci, 58(1), 7–25, 2001.
Dupuy, E., Urban, J., Ricaud, P., Le Flochmoën, É., Lautié, N., Murtagh, D., De La Noë, J., El Amraoui, L., Eriksson, P., Forkman, P., Frisk, U., Jégou, F., Jiménez, C., and Olberg, M: Strato-mesospheric measurements of carbon monoxide with the Odin Sub-Millimetre Radiometer: Retrieval and first results, Geophys. Res. Lett, 31, L20101, doi:10.1029/2004GL020558, 2004.
Eyring, V., Butchart, N., Waugh, D. W., et al.: Assessment of temperature, trace species, and ozone in chemistry-climate model simulations of the recent past, J. Geophys. Res., 111, D22308, doi:10.1029/2006JD007327, 2006.
Eyring, V., Waugh, D. W., Bodeker, G. E., et al.: Multi-model projections of stratospheric ozone in the 21st century. J. Geophys. Res., 112, D16303, doi:10.1029/2006JD008332, 2007.
Filipiak, M. J., Harwood, R. S., Jiang, J. H., Li, Q., Livesey, N. J., Manney, G. L., Read, W. G., Schwartz, M. J., Waters, J. W., and Wu, D. L.: Carbon monoxide measured by the EOS Microwave Limb Sounder on Aura: First results, Geophys. Res. Lett., 32, L14825, doi:10.1029/2005GL022765, 2005.
Folkins, I., Bernath, P., Boone, C., Lesins, G., Livesey, N., Thompson, A.M., Walker, K., and Witte, J.C.: Seasonal cycles of O_3, CO, and convective outflow at the tropical tropopause, Geophys. Res. Lett. 33, L16802, doi:10.1029/2006GL026602, 2006.
Fomichev V. I., Fu, C., de Grandpré, J., Beagley, S. R., Ogibalov, V. P., and McConnell, J. C.: Model thermal response to minor radiative energy sources and sinks in the middle atmosphere. J. Geophys. Res., 109, D19107, doi:10.1029/2004JD004892, 2004.
Fomichev V. I., Jonsson, A. I., de Grandpré, J., Beagley, S. R., McLandress, C., Semeniuk, K., and Shepherd, T. G.: Response of the Middle Atmosphere to CO_2 Doubling: Results from the Canadian Middle Atmosphere Model, J. Climate, 20(7), 1121–1144, 2007.
Forkman, P., Eriksson, P., Winnberg, A., Garcia, R. R., and D. Kinnison: Longest continuous ground-based measurements of mesospheric CO, Geophys. Res. Lett., 30(10), 1532,

doi:10.1029/2003GL016931, 2003.
Forkman P., Eriksson, P., Murtagh, D., and Espy, P.: Observing the vertical branch of the mesospheric circulation at latitude 60° N using ground-based measurements of CO and H_2O, J. Geophys. Res., 110, D05107, doi:10.1029/2004JD004916, 2005.
Froidevaux, L., Livesey, N. J., Read, W. G., et al.: Early validation analyses of atmospheric profiles from EOS MLS on the Aura satellite, IEEE Trans. Geosci. Remote Sensing, 44(5), 1106–1121, 2006.
Garcia, R. R., Dunkerton, T. J., Lieberman, R. S., and Vincent, R. A.: Climatology of the semi-annual oscillation of the tropical middle atmosphere, J. Geophys. Res., 102(D22), 26019–26032, 1997.
Gray, L. J. and Pyle, J. A.: The semi-annual oscillation and equatorial tracer distributions, Q. J. R. Meteor. Soc., 112, 387–407, 1986.
Hauchecorne, A., Bertaux, J.-L., Dalaudier, F., Russell, J. M., III, Mlynczak, M. G., Kyrölä, E., and Fussen, D.: Large increase of NO_2 in the north polar mesosphere in January–February 2004: Evidence of a dynamical origin from GOMOS/ENVISAT and SABER/TIMED data, Geophys. Res. Lett., 34, L03810, doi:10.1029/2006GL027628, 2007.
Hirota, I.: Equatorial Waves in the Upper Stratosphere and Mesosphere in Relation to the Semiannual Oscillation of the Zonal Wind, J. Atmos. Sci., 35(4), 714–722, 1978.
Holton, J. R.: The role of gravity wave induced drag and diffusion in the momentum budget of the mesosphere. J. Atmos. Sci., 39, 791–799, 1982.
Huang, F. T., Mayr, H. G., Reber, C. A., Russell, J. M., III, Mlynczak, M. G., and Mengel, J. G.: Ozone quasi-biennial oscillations (QBO), semiannual oscillations (SAO), and correlations with temperature in the mesosphere, lower thermosphere, and stratosphere, based on measurements from SABER on TIMED and MLS on UARS, J. Geophys. Res., 113, A01316, doi:10.1029/2007JA012634, 2008.
Intergovernmental Panel on Climate Change (IPCC), Climate Change 2001: The scientific basis. Contribution of Working Group 1 to the Third Assessment Report, edited by J. T. Houghton et al., Cambridge Univ. Press, New York, 2001.
Jin, J. J., Semeniuk, K., Jonsson, A. I., Beagley, S. R., McConnell, J. C., Boone, C. D., Walker, K. A., Bernath, P. F., Rinsland, C. P., Dupuy, E., Ricaud, P., De la Noe, J., Urban, J., and Murtagh, D.: Co-located ACE-FTS and Odin/SMR stratospheric-mesospheric CO 2004 measurements and comparison with a GCM, Geophys. Res. Lett., 32, L15S03, doi:10.1029/2005GL022433, 2005.

Jin, J. J., Semeniuk, K., Manney, G. L., Jonsson, A. I., Beagley, S. R., McConnell, J. C., Dufour, G., Nassar, R., Boone, C. D., Walker, K. A., Bernath, P. F., Rinsland, C. P.: Severe Arctic ozone loss in the winter 2004/2005: observations from ACE-FTS, Geophys. Res. Lett., 33, L15801, doi:10.1029/2006GL026752, 2006.

Jones, N. B., Kasai, Y., Dupuy, E., Murayama, Y., Urban, J., Barret, B., Sinnhuber, M., and Kagawa, A.: Stratomesospheric CO measured by a ground-based Fourier Transform Spectrometer over Poker Flat, Alaska: Comparisons with Odin/SMR and a 2-D model, J. Geophys. Res., 112, D20303, doi:10.1029/2006JD007916, 2007.

Jonsson A. I., de Grandpré, J., Fomichev, V. I., McConnell, J. C., and Beagley, S. R.: Doubled CO_2-induced cooling in the middle atmosphere: Photochemical analysis of the ozone radiative feedback, J. Geophys. Res., 109, D24103, doi:10.1029/2004JD005093, 2004.

Juckes, M. N.: An annual cycle of long lived stratospheric gases from MIPAS, Atmos. Chem. Phys., 7, 1879–1897, 2007, http://www.atmos-chem-phys.net/7/1879/2007/.

Lambert, A., Read, W. G., Livesey, N. J., et al.: Validation of the Aura Microwave Limb Sounder middle atmosphere water vapor and nitrous oxide measurements, J. Geophys. Res., 112, D24S36, doi:10.1029/2007JD008724, 2007.

Liu, C., Zipser, E., Garrett, T., Jiang, J. H., and Su, H.: How do the water vapor and carbon monoxide "tape recorders" start near the tropical tropopause?, Geophys. Res. Lett., 34, L09804, doi:10.1029/2006GL029234, 2007.

Livesey, N. J., Filipiak, M. J., Froidevaux, L., et al.: Validation of Aura Microwave Limb Sounder O_3 and CO observations in the upper troposphere and lower stratosphere, J. Geophys. Res. 113, D15S02, doi:10.1029/2007JD008805, 2008.

López-Valverde, M. A, López-Puertas, M., Remedios, J. J., Rodgers, C. D., Taylor, F. W., Zipf, E. C., and Erdman, P. W.: Validation of measurements of carbon monoxide from the improved stratospheric and mesospheric sounder, J. Geophys. Res. 101(D6), 9929–9956, 1996.

Manney, G. L., Zurek, R. W., O'Neill, A., and Swinbank, R.: On the motion of air through stratospheric polar vortex, J. Atmos. Sci., 51, 2973–2994, 1994.

Manney, G. L., Zurek, R. W., Lahoz, W. A., Harwood, R. S., Kumer, J. B., Mergenthaler, J., Roche, A. E., O'Neill, A., Swinbank, R., and Waters, J. W.: Lagrangian transport calculations using UARS data. Part I: Passive tracers, J. Atmos. Sci. 52, 3049–3068, 1995.

Manney, G. L., Krüger, K., Sabutis, J. L., Sena, S. A., and Pawson, S.: The remarkable 2003–2004 winter and other recent warm winters in the Arctic stratosphere since the late 1990s, J.

Geophys. Res., 110, D04107, doi:10.1029/2004JD005367, 2005a.
Manney G. L., Santee, M. L., Livesey, N. J., Froidevaux, L., Read, W. G., Pumphrey, H. C., Waters, J. W., and Pawson, S.: EOS Microwave Limb Sounder observations of the Antarctic polar vortex breakup in 2004, Geophys. Res. Lett., 32, L12811, doi:10.1029/2005GL022823, 2005b.
Manney, G. L., Santee, M. L., Froidevaux, L., Hoppel, K., Livesey, N. J., and Waters, J. W.: EOS MLS observations of ozone loss in the 2004–2005 Arctic winter, Geophys. Res. Lett., 33, L04802, doi:10.1029/2005GL024494, 2006.
Manney, G. L., Daffer, W. H., Zawodny, J. M., et al.: Solar Occultation Satellite Data and Derived Meteorological Products: Sampling Issues and Comparisons with Aura MLS, J. Geophys. Res. 112, D24S50, doi:10.1029/2007JD008709, 2007.
Manney, G. L., Daffer, W. H., Strawbridge, K. B., et al.: The High Arctic in Extreme Winters: Vortex, Temperature, and MLS and ACE-FTS Trace Gas Evolution, Atmos. Chem. Phys. 8, 505–522, 2008a.
Manney, G. L., Krueger, K., Pawson, S., Minschwaner, K., Schwartz, M. J., Daffer, W., Livesey, N. J., Mlynczak, M. G., Remsberg, E., Russell, J. M., and Waters, J. W.: The evolution of the stratopause during the 2006 major warming: Satellite Data and Assimilated Meteorological Analyses, J. Geophys. Res., 113, D11115, doi:10.1029/2007JD009097, 2008b.
Medvedev, A. S. and Klaassen, G. P: Realistic Semiannual Oscillation Simulated in a Middle Atmosphere General Circulation Model, Geophys. Res. Lett., 28(4), 733–736, 2001.
Mote, P. W., Rosenlof, K. H., McIntyre, M. E., Carr, E. S., Gille, J. C., Holton, J. R., Kinnersley, J. S., Pumphrey, H. C., Russell, J. M., III, and Waters, J. W.: An atmospheric tape recorder: The imprint of tropical tropopause temperatures on stratospheric water vapor, J. Geophys. Res., 101(D2), 3989–4006, 1996.
Murtagh, D., Frisk, U., Merino, F., et al.: An overview of the Odin atmospheric mission, Can. J. Phys., 80(4), 309–319, 2002.
Plumb, R. A.: Stratospheric transport, J. Meteor. Soc. Japan, 80, 793–809, 2002.
Plumb, R. A., Heres, W., Neu, J. L., Mahowald, N. M., del Corral, J., Toon, G. C., Ray, E., Moore, F., and Andrews, A. E.: Global tracer modeling during SOLVE: High-latitude descent and mixing, J. Geophys. Res., 107, 8309, doi:10.1029/2001JD001023, 2002, [printed 108(D5), 8309, 2003].
Polavarapu S., Ren, S. Z., Rochon, Y., Sankey, D., Ek, N., Koshyk, J., and Tarasick, D.: Data assimilation with the Canadian middle atmosphere model, Atmos. Ocean, 43(1), 77–100,

2005.
Pumphrey, H. C., Filipiak, M. J., Livesey, N. J., Schwartz, M. J., Boone, C., Walker, K. A., Bernath, P., Ricaud, P., Barret, Clerbaux, C., Jarnot, R. F., Manney, G. L., and Waters, J. W.: Validation of middle-atmosphere carbon monoxide retrievals from MLS on Aura, J. Geophys. Res., 112, D24S38, doi:10.1029/2007JD008723, 2007.
Pumphrey H. C., Boone, C., Walker, K. A., Bernath, P., and Livesey, N. J.:, Tropical tape recorder observed in HCN, Geophys. Res. Lett., 35, L05801, doi:10.1029/2007GL032137, 2008.
Randall, C. E., Harvey, V. L., Singleton, C. S., Bernath, P. F., Boone, C. D., and Kozyra, J. U.: Enhanced NO_x in 2006 linked to strong upper stratospheric Arctic vortex, Geophys. Res. Lett., 33, L18811, doi:10.1029/2006GL027160, 2006.
Randel, W. J. and Wu, F.: Isolation of the Ozone QBO in SAGE II Data by Singular-Value Decomposition, J. Atmos. Sci., 53(17), 2546–2559, 1996.
Randel, W. J., Wu, F., Russell, J. M., III, Roche, A., and Waters, J. W.: Seasonal Cycles and QBO Variations in Stratospheric CH_4 and H_2O Observed in UARS HALOE Data, J. Atmos. Sci., 55, 163–185, 1998.
Randel, W. J., Wu, F., Gettelman, A., Russell III, J. M., Zawodny, J. M., and Oltmans, S. J.: Seasonal variation of water vapor in the lower stratosphere observed in Halogen Occultation Experiment data, J. Geophys. Res., 106(13), 14 313–14 325, 2004.
Randel, W. J., Park, M., Wu, F., and Livesey, N. J.: A large annual cycle in ozone above the tropical tropopause linked to the Brewer-Dobson circulation, J. Atmos. Sci., 64, 4479–4488, 2007.
Ray, E., Holton, J. R., Fishbein, E. F., Froidevaux, L., and Waters, J. W.: The tropical semiannual oscillation in temperature and ozone observed by the MLS, J. Atmos. Sci., 51, 3045–3052, 1994.
Read, W. G., Wu, D. L., Waters, J. W., and Pumphrey, H. C.: Dehydration in the tropical tropopause layer: Implications from the UARS Microwave Limb Sounder, J. Geophys. Res., 109, D06110, doi:10.1029/2003JD004056, 2004.
Rinsland, C. P., Boone, C., Nassar, R., Walker, K., Bernath, P., McConnell, J. C., and Chiou, L.: Atmospheric Chemistry Experiment (ACE) Arctic stratospheric measurements of NO_x during February and March 2004: Impact of intense solar flares, Geophys. Res. Lett., 32, L16S05, doi:10.1029/2005GL022425, 2005.
Rösevall, J. D., Murtagh, D. P., and Urban, J.: Ozone depletion in the 2006/2007 Arctic winter,

Geophys. Res. Lett., 34, L21809, doi:10.1029/2007GL030620, 2007.
Russell, J. M., III, Gordley, L. L., Park, J. H., Drayson, S. R., Hesketh, W. D., Cicerone, R. J., Tuck, A. F., Frederick, J. E., Harries, J. E., and Crutzen, P. J.: The Halogen Occultation Experiment, J. Geosphys. Res., 98(D6), 10 777–10 797, 1993.
Ruth, S., Kennaugh, R., Gray, L. J., and Russell III, J. M.: Seasonal, semiannual, and interannual variability seen in measurements of methane made by the UARS Halogen Occultation Experiment, J. Geophys. Res., 102(D13), 16 189–16 199, 1997.
Schoeberl, M. R., Lait, L. R., Newman, P. A., and Rosenfield, J. E.: The Structure of the Polar Vortex, J. Geophys. Res., 97(D8), 7859–7882, 1992.
Schoeberl, M. R, Luo, M., and Rosenfield, J. E.: An analysis of the Antarctic Halogen Occultation Experiment trace gas observations, J. Geophys. Res., 100(D3), 5159–5172, 1995.
Schoeberl, M. R., Duncan, B. N., Douglass, A. R., Waters, J., Livesey, N., Read, W., and Filipiak, M.: The carbon monoxide tape recorder, Geophys. Res. Lett., 33, L12811, doi:10.1029/2006GL026178, 2006.
Schoeberl, M. R., Douglass, A. R., Newman, P. A., Lait, L. R., Lary, D., Waters, J., Livesey, N., Froidevaux, L., Lambert, A., Read, W., Filipiak, M. J., and Pumphrey, H. C.: QBO and Annual Cycle Variations in Tropical Lower Stratosphere Trace Gases from HALOE and Aura MLS Observations, J. Geophys. Res. 113, D05301, doi:10.1029/2007JD008678, 2008.
Semeniuk, K., McConnell, J. C., Jin, J. J., Jarosz, J. R., Bernath, P. F., and Boone, C. D.: N_2O production by high energy auroral electron precipitation, J. Geophys. Res., doi:10.1029/2007JD009690, in press, 2008.
Shepherd, T. G.: The middle atmosphere, J. Atmos. Solar-Terres. Phys., 62, 1587–1601, 2000.
Shepherd, T. G. and Jonsson, A. I.: On the attribution of stratospheric ozone and temperature changes to changes in ozone depleting substances and well mixed greenhouse gases, Atmos. Chem. Phys., 8, 1435–1444, 2008, http://www.atmos-chem-phys.net/8/1435/2008/.
Shepherd, T. G.: Transport in the middle atmosphere, J. Meteor. Soc. Japan, 85B, 165–191, 2007.
Siskind, D. E., Eckermann, S. D., Coy, L., McCormack, J. P., and Randall, C. E.: On recent interannual variability of the Arctic winter mesosphere: Implications for tracer descent, Geophys. Res. Lett., 34, L09806, doi:10.1029/2007GL029293, 2007.
Strong, K., Wolff, M. A., Kerzenmacher, T. E., Walker, K. A., Bernath, P. F., et al.:, Validation of ACE-FTS N_2O measurements, Atmos. Chem. Phys. Discuss., 8, 3597–3663, 2008,

http://www.atmos-chem-phys-discuss.net/8/3597/2008/.
Tian W., Chipperfield, M. P., Gray, L. J., and Zawodny, J. M.: Quasi-biennial oscillation and tracer distributions in a coupled chemistry-climate model, J. Geophys. Res., 111, D20301, doi:10.1029/2005JD006871, 2006.
Urban, J., Lautié, N., Le Flochmoën, E., et al.: Odin/SMR limb observations of stratospheric trace gases: Validation of N_2O, J. Geophys. Res., 110, D09301, doi:10.1029/2004JD005394, 2005.
Urban, J., Murtagh, D. P., Lautié, N., et al.: Odin/SMR Limb Observations of Trace Gases in the Polar Lower Stratosphere during 2004–2005, Proc. ESA First Atmospheric Science Conference, 8–12 May 2006, Frascati, Italy/Ed. Lacoste, H., ESA-SP-628 Noordwijk: European Space Agency. ISBN/ISSN: ISBN-92-9092-939-1, ISSN-1609-042X, 2006.
Velazco, V., Wood, S. W., Sinnhuber, M., Kramer, I., Jones, N. B., Kasai, Y., Notholt, J., Warneke, T., Blumenstock, T., Hase, F., Murcray, F. J., and Schrems, O.:, Annual variation of strato-mesospheric carbon monoxide measured by ground-based Fourier transform infrared spectrometry, Atmos. Chem. Phys., 7, 1305–1312, 2007, http://www.atmos-chem-phys.net/7/1305/2007/.
Waters, J. W., Froidevaux, L., Harwood, R. S., et al.: The Earth Observing System Microwave Limb Sounder (EOS MLS) on the Aura satellite, IEEE Trans. Geosci. Remote Sensing, 44(5), 1075–1092, 2006.
World Meteorological Organization (WMO): Scientific Assessment of Ozone Depletion: 2002, Global Ozone Research and Monitoring Project–Report No. 47, Geneva, 2003.
World Meteorological Organization (WMO): Scientific Assessment of Ozone Depletion: 2006, Global Ozone Research and Monitoring Project–Report No. 50, Geneva, 2007.
Zhang, X. C.: The semi-annual oscillation in the middle atmosphere: A comparison of CMAM with HALOE measurements, M. Sc. dissertation, York University, Canada, 2002.

Table 1. Availability of Odin/SMR v225 CO data.

Year	Jan.	Feb.	Mar.	Apr.	May	Jun.	Jul.	Aug.	Sep.	Oct.	Nov.	Dec.
2003										8–9	13–14; 30–	1; 19–20
2004	10–11 29–30	15–16	5–6; 22–23	27–28	16–17	21–22	27–28	13–14; 19–20; 25–26	1–2; 18–19		29–30	
2005		23–24										
2006	13–18; 21–22; 24–25; 27–28; 30–31	1–2						31				

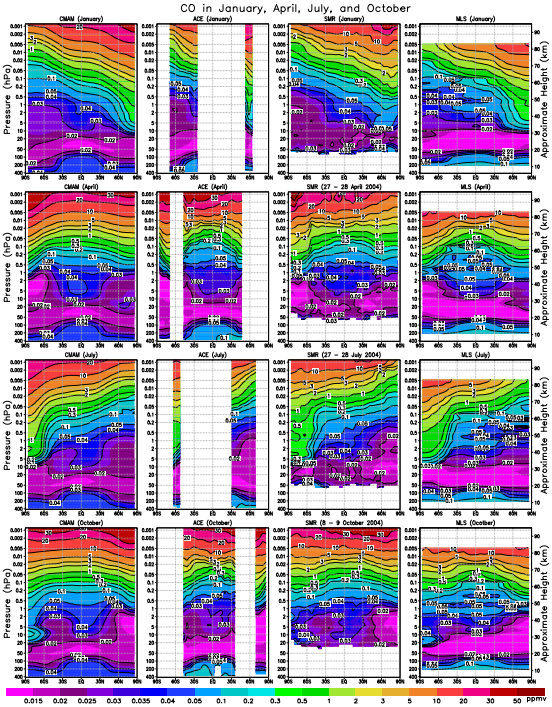

Fig. 1. Monthly zonal mean latitude-pressure cross-sections of CO from CMAM, ACE-FTS, SMR, and MLS.

ACPD
8, 13063–13123, 2008

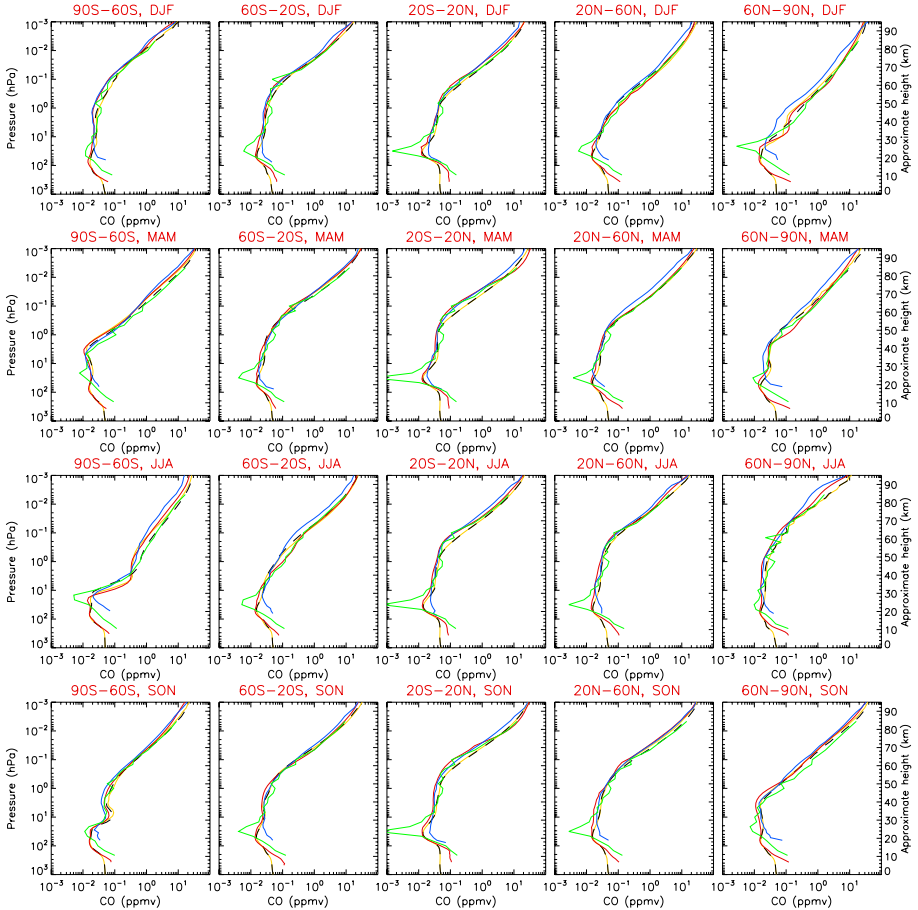

Fig. 2. Seasonal mean CO profiles. Black dash line, CMAM simulations; yellow solid line, CMAM simulations near the ACE-FTS latitudes; blue solid line, SMR measurement; green solid line, MLS measurements; red solid line, ACE-FTS measurements.

ACPD
8, 13063–13123, 2008

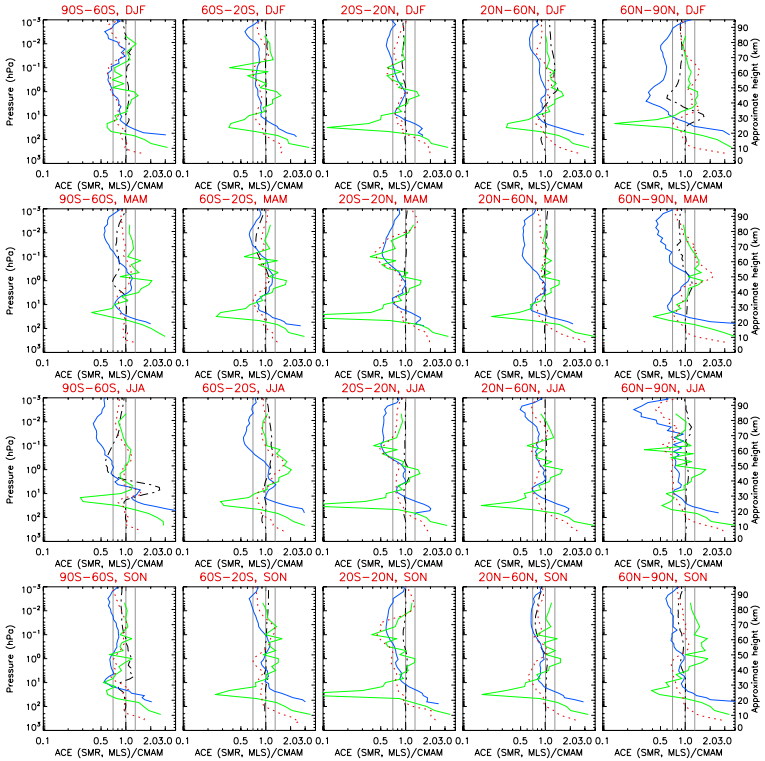

Fig. 3. Ratios for seasonal mean CO profiles. Blue solid line, SMR/CMAM; green solid line, MLS/CMAM; red dot line, ACE-FTS/(CMAM near the ACE-FTS latitudes); black dash-dot line, (CMAM sampled near the ACE-FTS latitudes)/CMAM. Blue dash line, ACE-FTS/(CMAM near the ACE-FTS latitudes) for N_2O, which is shown in the FIg. 6. The grey vertical straight lines indicate ratios 0.7, 1.0 and 1.3. The values of the measurements and the model results are shown in Fig. 2.

ACPD
8, 13063–13123, 2008

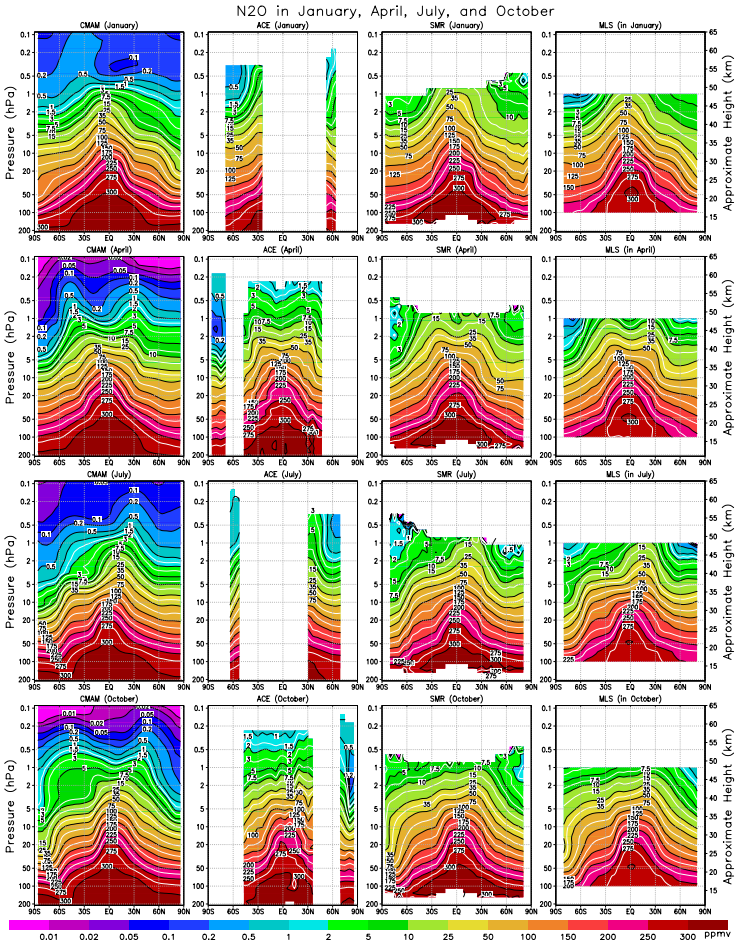

Fig. 4. Monthly zonal mean latitude-pressure cross-sections of N_2O from CMAM, ACE-FTS, SMR, and MLS.

ACPD
8, 13063–13123, 2008

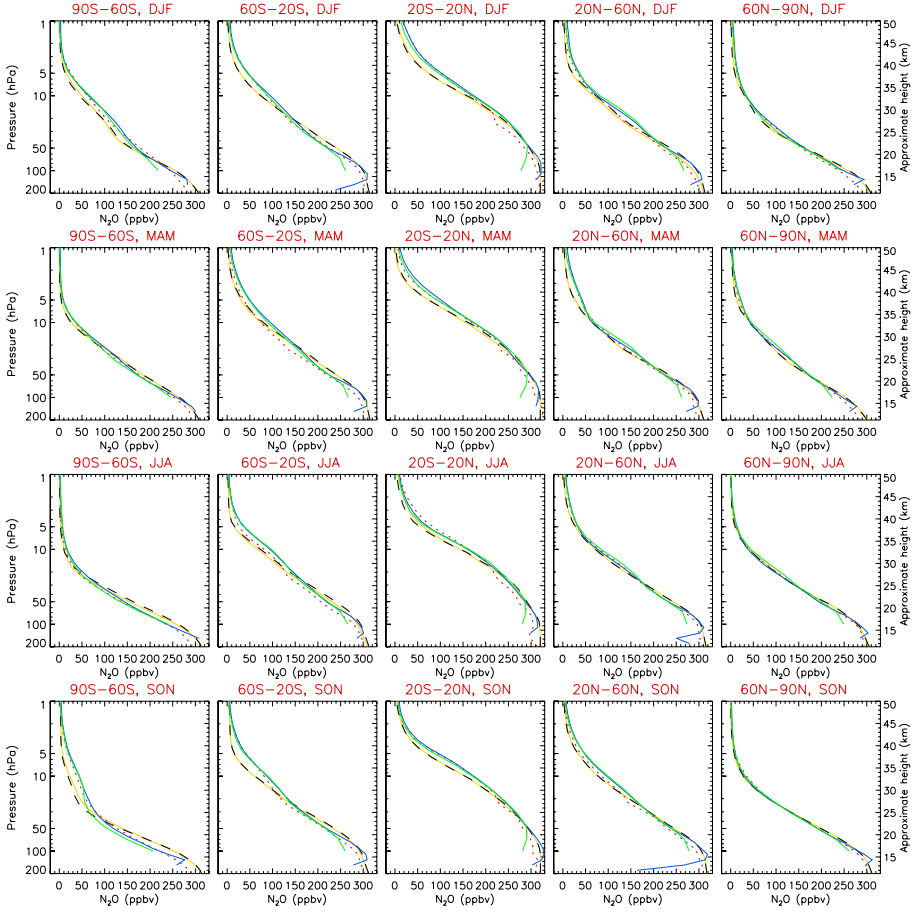

Fig. 5. Seasonal mean N_2O profiles. See the colour scheme in Fig 2.

ACPD
8, 13063–13123, 2008

Comparison of CMAM with SMR, ACE-FTS, and MLS

J. J. Jin et al.

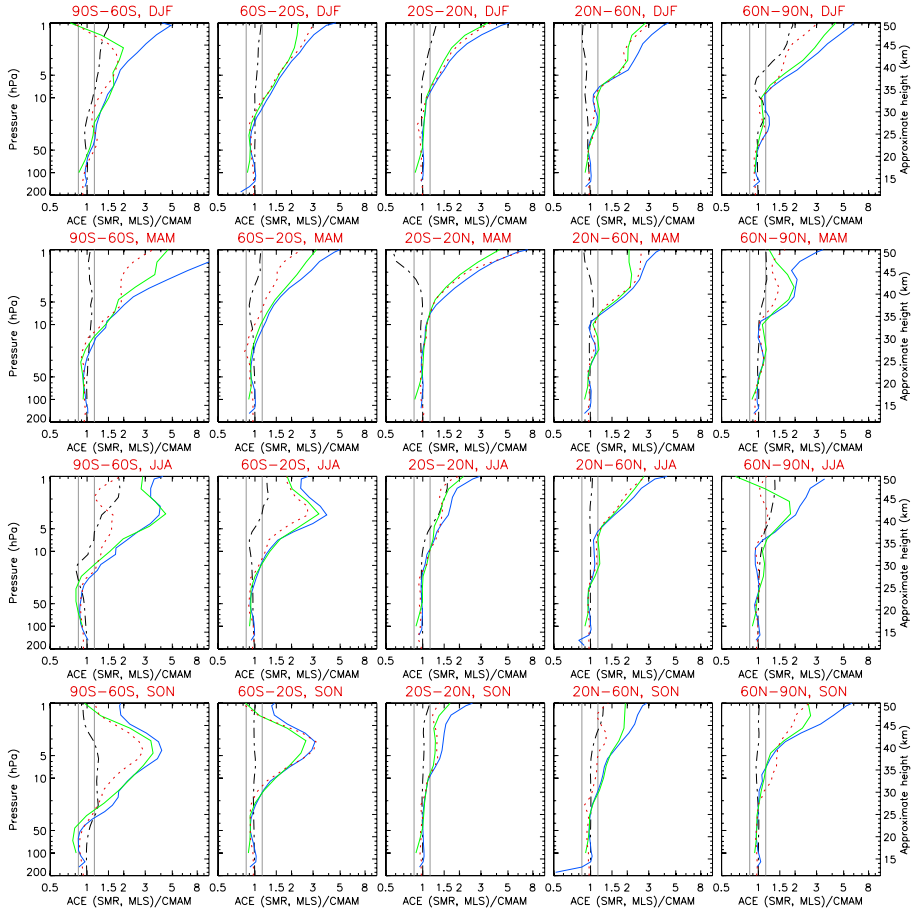

Fig. 6. Ratios for seasonal mean N_2O profiles. See the colour scheme in Fig. 3. The grey vertical straight lines indicate ratios 0.85 and 1.15. The values of the measurements and the model results are shown in Fig. 5.

ACPD
8, 13063–13123, 2008

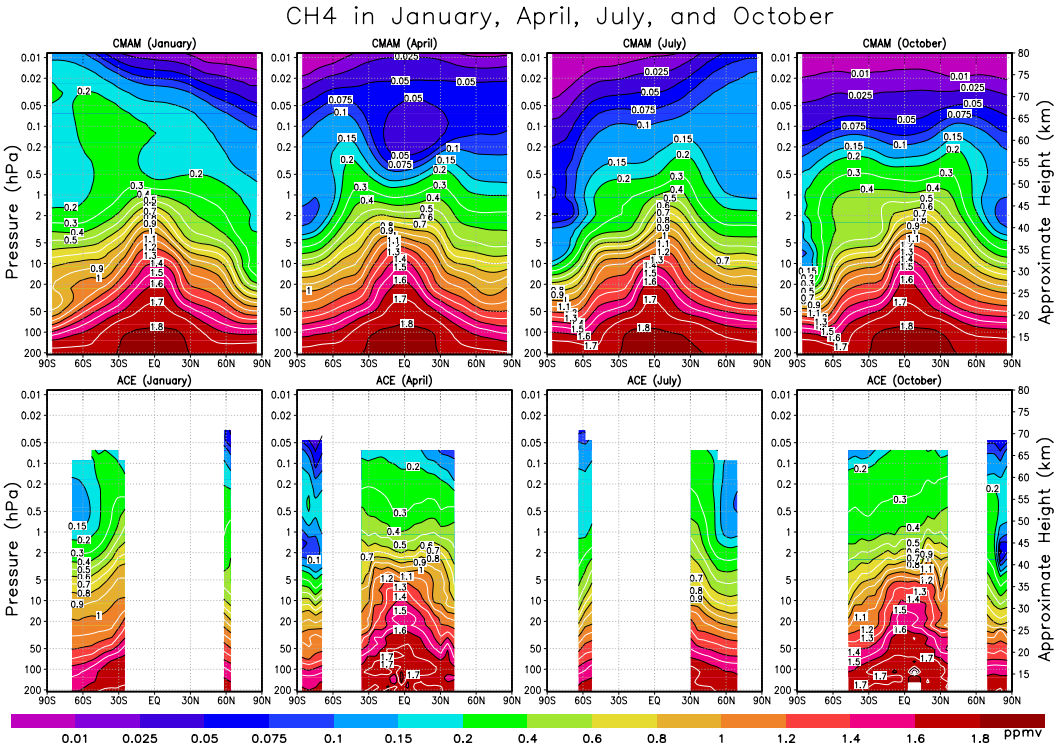

Fig. 7. Monthly zonal mean latitude-pressure cross-sections of CH_4 from CMAM and ACE-FTS.

ACPD
8, 13063–13123, 2008

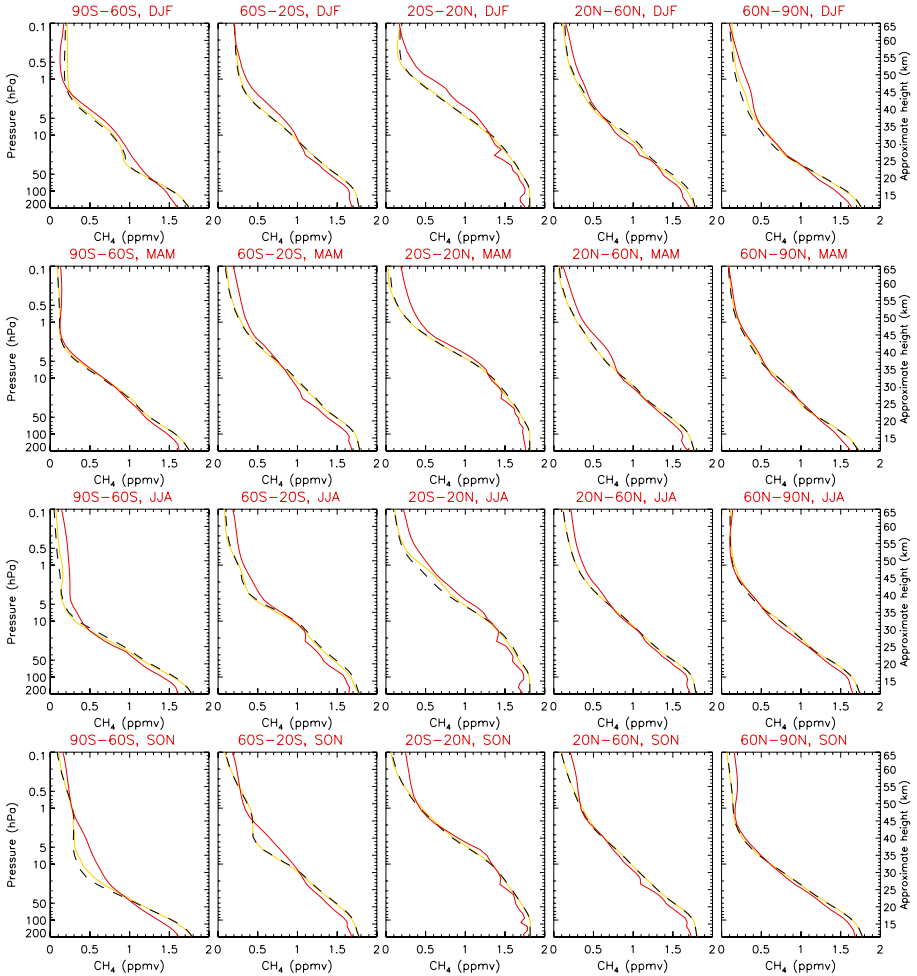

Fig. 8. Seasonal zonal mean CH_4 profiles. See the colour scheme in Fig. 2.

ACPD
8, 13063–13123, 2008

Comparison of CMAM with SMR, ACE-FTS, and MLS

J. J. Jin et al.

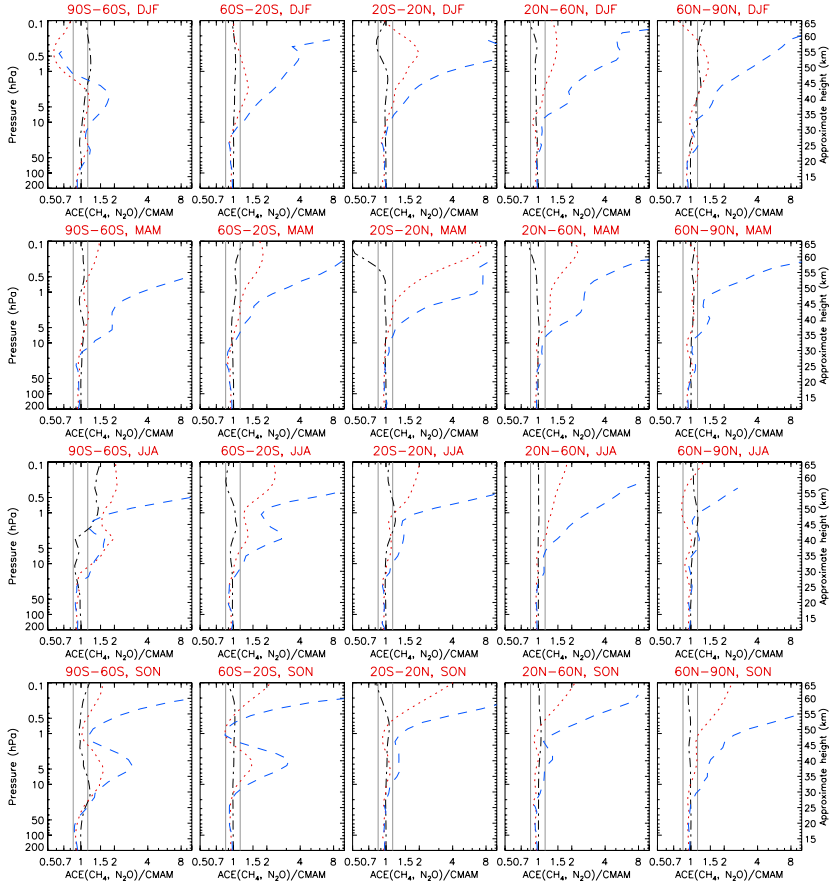

Fig. 9. Ratios for seasonal mean CH_4 profiles. See the colour scheme in Fig. 3. Blue dash line, ACE-FTS/(CMAM near the ACE-FTS latitudes) for N_2O, which is shown in the Fig. 6. The grey vertical straight lines indicate ratios 0.85 and 1.15. The values of the measurements and the model results are shown in Fig. 8.

ACPD
8, 13063–13123, 2008

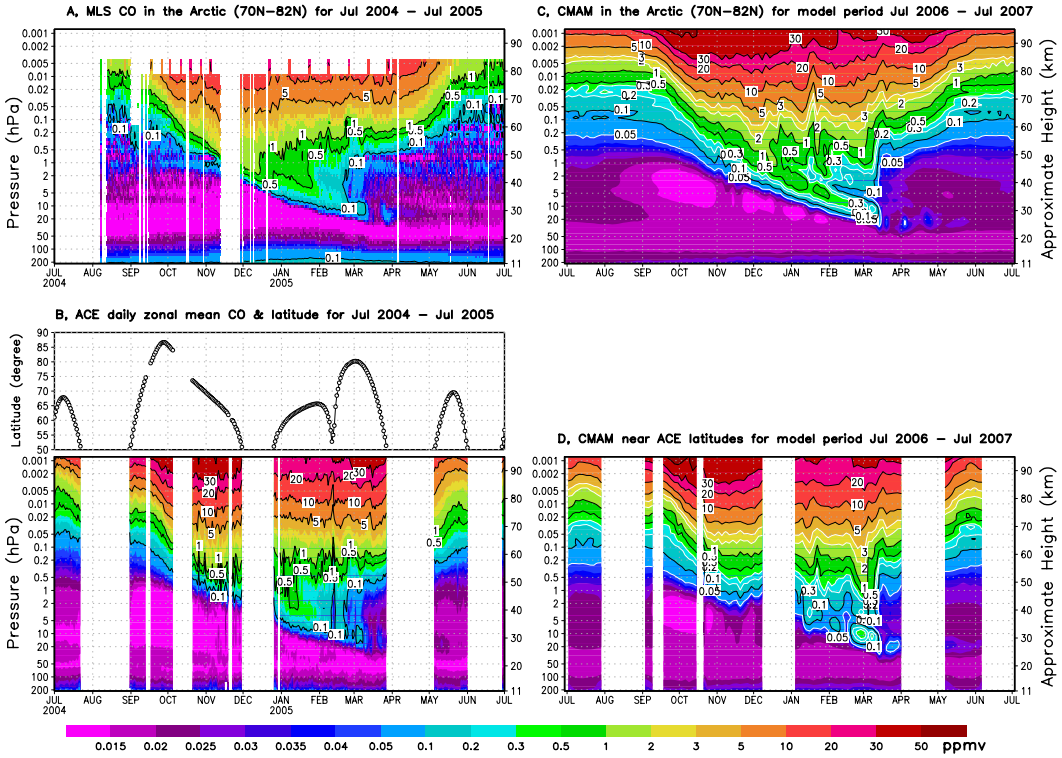

Fig. 10. Evolution of CO zonal averages from MLS (panel A) and ACE-FTS (panel B) measurements for the period 1 July 2004–1 July 2005. CMAM results and CMAM results near the ACE-FTS latitudes in the Arctic for the model period 1 July 2006–1 July 2007 are shown in panel C and panel D, respectively. The averaged latitudes of ACE-FTS are also shown in panel B.

ACPD
8, 13063–13123, 2008

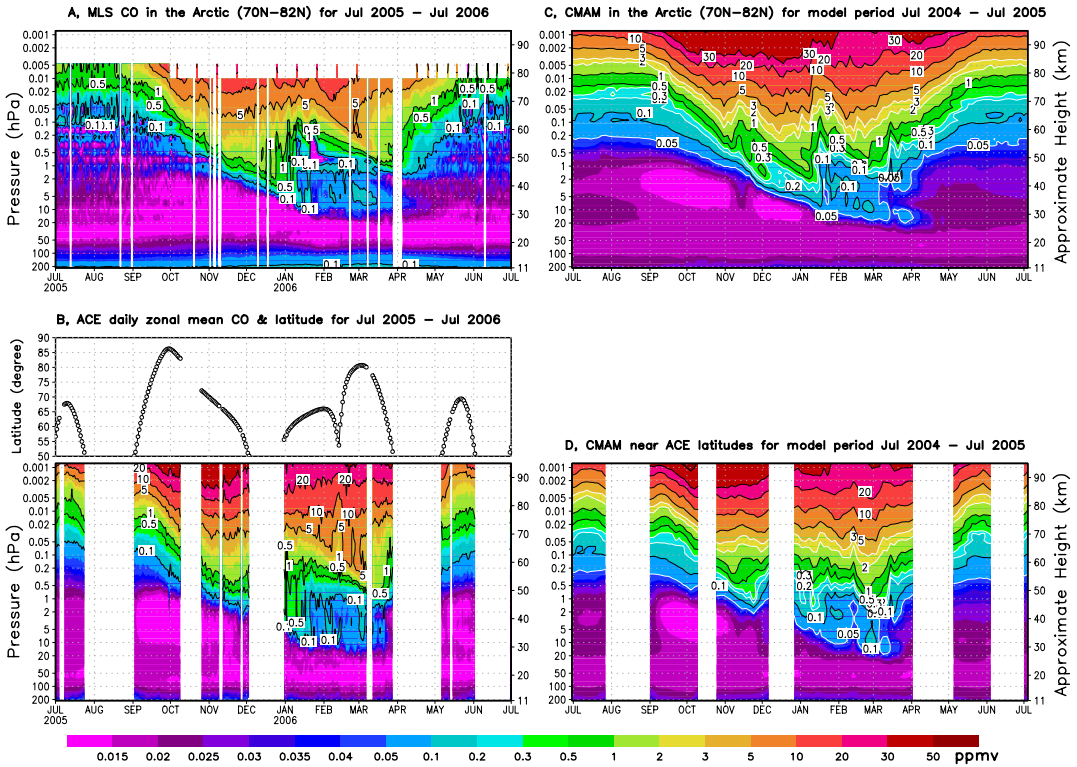

Fig. 11. Evolution of CO zonal averages. See the panel scheme in Fig. 10, but the observation period of MLS and ACE-FTS is 1 July 2005–1 July 2006 and the model period is 1 July 2004–1 July 2005.

ACPD
8, 13063–13123, 2008

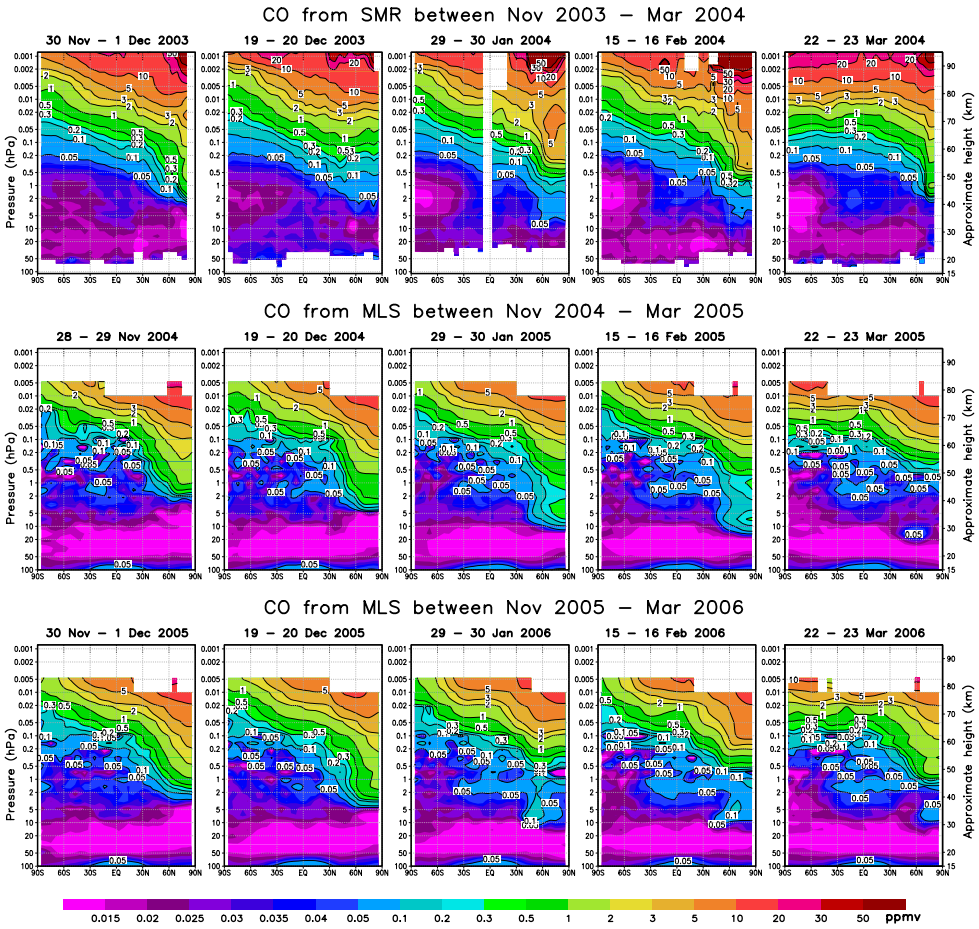

Fig. 12. Latitude-pressure cross-sections of CO measurements from SMR and MLS during the Arctic winters 2004, 2005, and 2006.

ACPD
8, 13063–13123, 2008

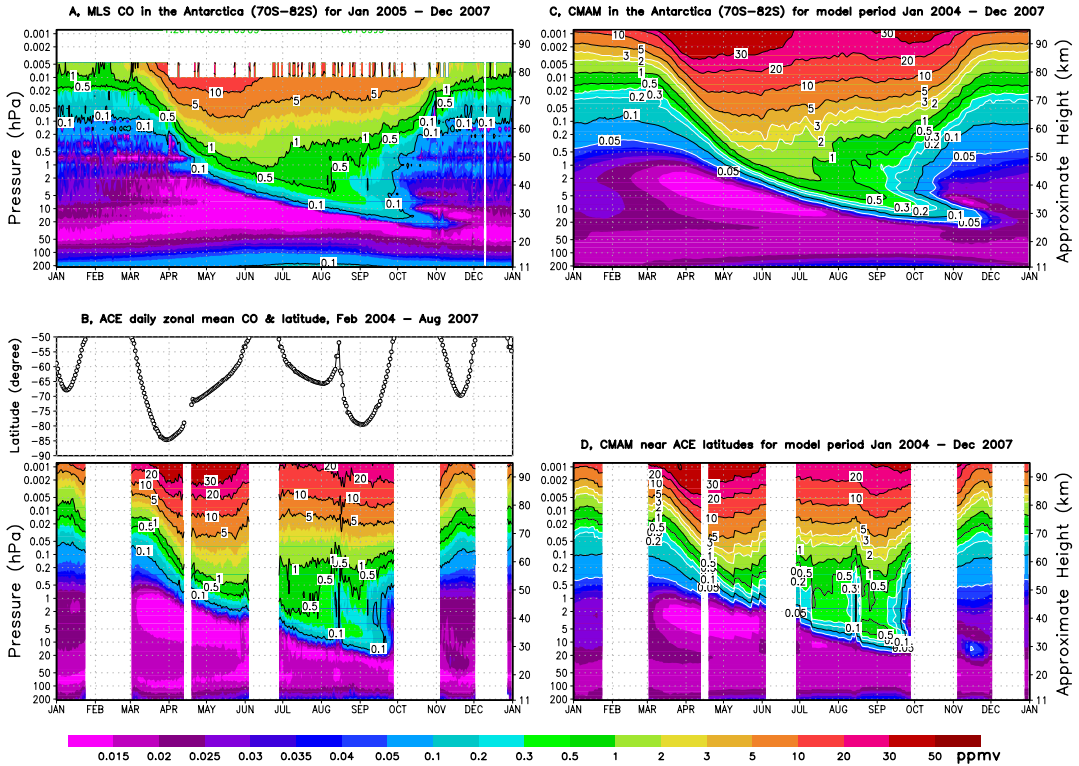

Fig. 13. Evolution of CO zonal averages from MLS and ACE-FTS measurements, CMAM results, and CMAM results at the ACE-FTS latitudes in the Antarctica.

ACPD
8, 13063–13123, 2008

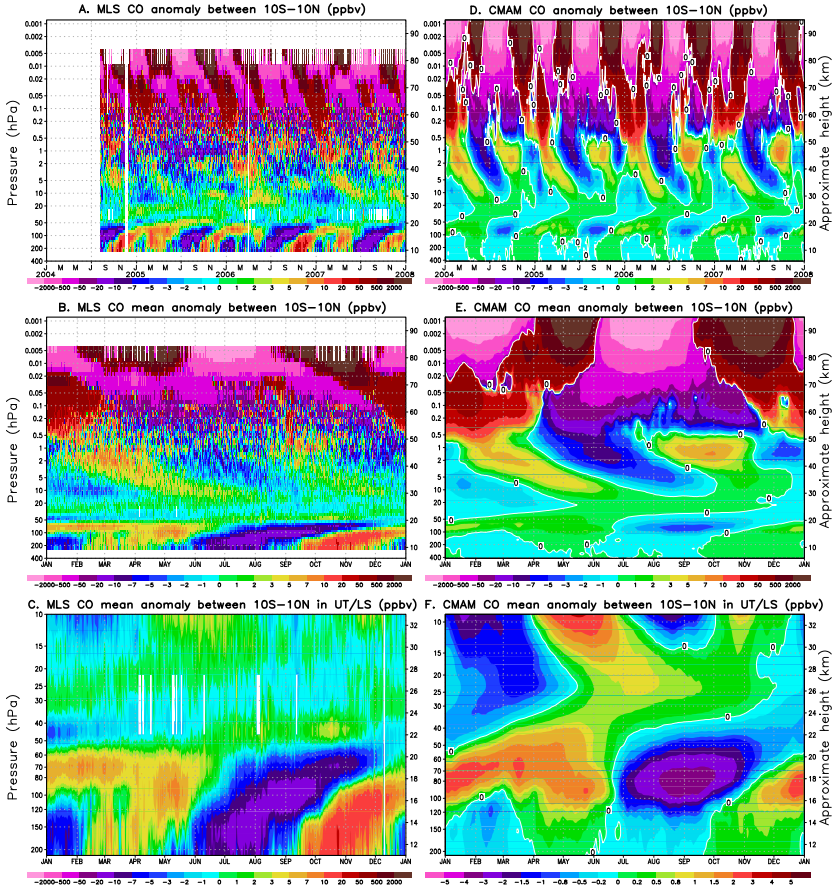

Fig. 14. Tropical CO anomalies (zonal means over annual averages) of MLS (panel A) and CMAM (panel D). Panel B and panel E show the mean anomalies. Panels C and panel F show the mean anomalies in the upper troposphere and lower stratosphere (UT/LS). Note the contour levels in panel F are different from the others.

ACPD
8, 13063–13123, 2008

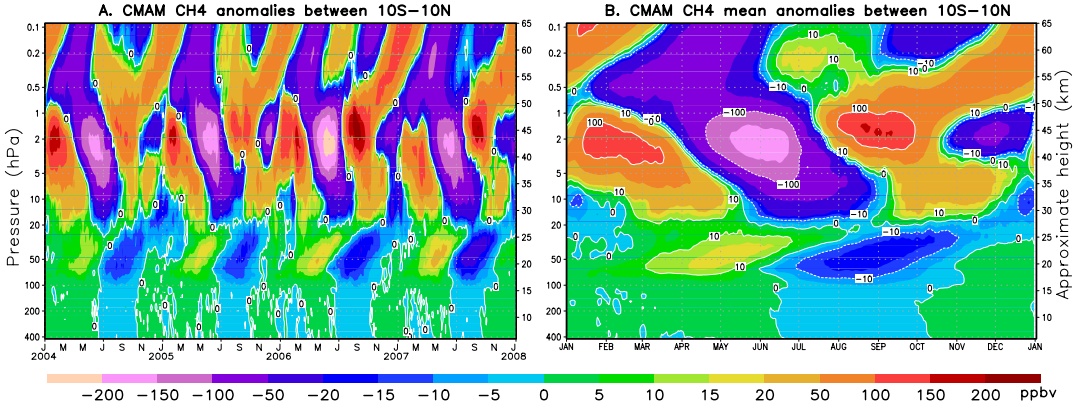

Fig. 15. Tropical CH_4 anomaly of CMAM (panel A) and its annual mean (panel B).

ACPD
8, 13063–13123, 2008

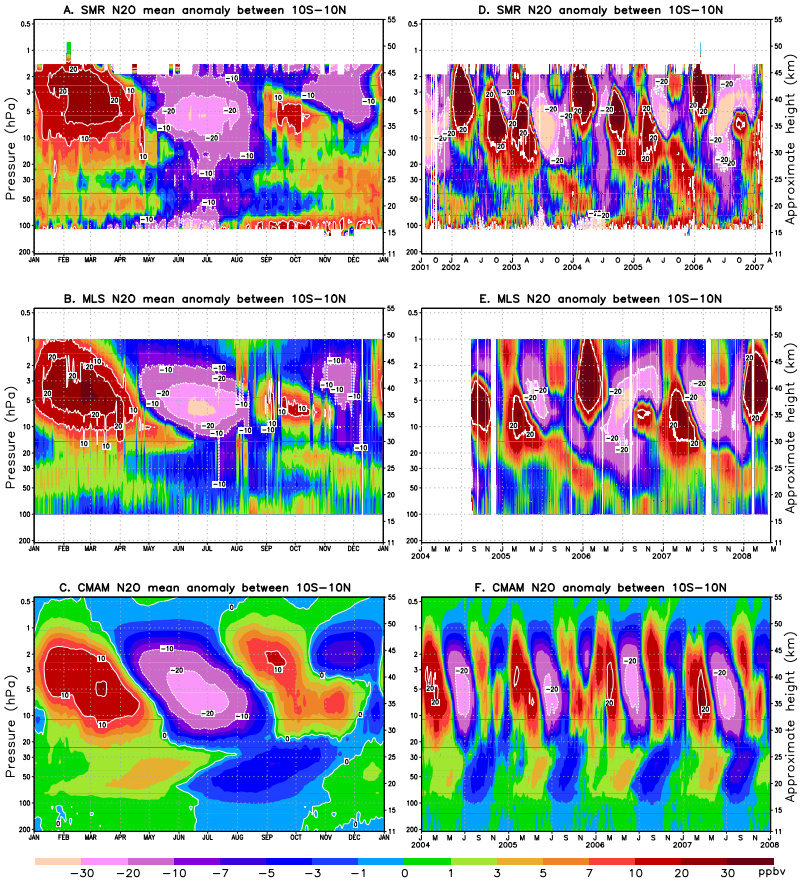

Fig. 16. Tropical N_2O mean anomalies of SMR (panel A), MLS (panel B) and CMAM (panel C). Panels D, E and F show the anomalies over long-term (periods shown in the plots) averages.

ACPD
8, 13063–13123, 2008